Chapter 20

Photosynthesis in Global-Scale Models

Andrew D. Friend*
Department of Geography, University of Cambridge, Downing Place, Cambridge CB2 3EN, UK

Richard J. Geider
Department of Biological Sciences, University of Essex, Wivenhoe Park, Colchester CO4 3SQ, UK

Michael J. Behrenfeld
Department of Botany and Plant Pathology, Oregon State University, Cordley Hall, 2082, Corvallis, OR 97331, USA

Christopher J. Still
Department of Geography and Institute for Computational Earth System Science, University of California Santa Barbara, Santa Barbara, CA 93106, USA

* Author for correspondence, e-mail: adf10@cam.ac.uk

A. Laisk, L. Nedbal and Govindjee (eds.), Photosynthesis in silico: Understanding Complexity from Molecules to Ecosystems, pp. 465–497.

Summary

Photosynthesis models are now routinely used in many types of global investigations. Much of this work is driven by global environmental change concerns, with global models seen as key tools with which to synthesize current understanding, explain paleoclimatic variability in global biogeochemistry and ecology, and forecast ecosystem responses to climate change and increasing atmospheric CO_2 levels. We discuss the approaches used to model terrestrial and marine photosynthesis at the global scale. Models in both realms fall into two equivalent categories, one empirical and one mechanistic. Within each category there are many similarities between terrestrial and marine models. Most empirical approaches estimate the distribution of photosynthetic capacity (chlorophyll in the oceans, LAI on land) from space and apply a photosynthetic light-use efficiency approach to obtain an estimate of carbon uptake. Mechanistic approaches attempt to simulate the distribution of capacity itself, as well as the rate of photosynthesis, and are thus capable of projecting terrestrial and marine carbon fluxes into the future and distant past.

A completely new state-of the-art global combined simulation of terrestrial and marine production is presented. Terrestrial photosynthesis is calculated using a mechanistic approach that treats the within-leaf light gradient, among other improvements over previous methods. Marine production utilizes a new approach that treats spatial and temporal variation in phytoplankton chlorophyll to C ratio. Mean contemporary annual net primary productivity is estimated to be 107.3 Pg C $year^{-1}$, with 51.1% coming from land and 48.9% from the oceans.

Improvements in prognostic modeling of global photosynthesis will come about through attention to the same issues in both terrestrial and marine environments. These primarily concern high quality validation data at scales appropriate to test global models and the development of methodologies to deal with the variety of physiological and phenological types. In addition, attention needs to be given to both the potential importance of phenotypic plasticity and better mechanistic approaches for the prediction of photosynthetic capacity distribution in space and time. Dialogue between modelers, experimental physiologists, and ecologists needs to improve. Without this there is a very real danger that global models will assume a shared acceptance of an *in silico* reality that bears only superficial resemblance to that *in vivo*.

Abbreviations: AOD – atmospheric optical depth; APAR – absorbed PAR; AVHRR – advanced very high resolution radiometer; CASA – Carnegie Ames Stanford approach; CbPM – carbon-based production model; *Chl* – chlorophyll *a* concentration; Chl *a* – chlorophyll *a*; C_{phyto} – ocean carbon concentration; DGOM – dynamic green ocean model; DGVM – dynamic global vegetation model; E_0 – incident PAR at the sea surface; f_{PAR} – fraction of PAR; GCM – global climate model; GPP – gross primary production; LAI – leaf area index; LUE – light use efficiency; MLD – mixed layer depth; MODIS – moderate-resolution imaging spectroradiometer; NDVI – normalized difference vegetation index; NIR – near infrared; NOAA – National Oceanic and Atmospheric Administration; NPP – net primary production; P^{Chl} – chlorophyll *a*-specific photosynthesis rate; $P(z, t)$ – depth and time resolved net carbon fixation rate per unit volume; PAR – photosynthetically active radiation; Rubisco – ribulose 1,5-bisphosphate carboxylase/oxygenase; RuBP – ribulose 1,5-bisphosphate; SeaWiFS – sea-viewing wide field-of-view sensor; *SLA* – specific leaf area

I. Introduction

All food and fiber on which humanity depends has its origin in the capture of atmospheric CO_2 by photosynthesis, and so quantifying present and future global spatial and temporal distributions of this essential process is a key scientific objective. Recent increases in computing power, together with the production of key global datasets, have allowed many researchers to develop methodologies for modeling photosynthesis at the global scale in both the terrestrial (Melillo et al., 1993; Potter et al., 1993; Warnent et al., 1994; Prince and Goward, 1995; VEMAP Members, 1995; Foley et al., 1996; Hunt et al., 1996; Kaduk and Heimann, 1996; Sellers et al., 1996a; Brovkin et al., 1997; Post et al., 1997; Dickinson et al., 1998; Xiao et al., 1998; Cox et al., 2000; Friend and White, 2000; McGuire et al., 2001; Bonan et al., 2003; Sitch et al., 2003; Running et al., 2004; Woodward and Lomas, 2004; Friend and Kiang, 2005; Krinner et al., 2005; Sato et al., 2007) and marine (Morel, 1991; Longhurst et al., 1995; Behrenfeld and Falkowski, 1997a; Behrenfeld et al., 2005; Carr et al., 2006) environments. These efforts have been driven by three ambitious research objectives: (i) synthesis of our understanding of the current ecological and biogeochemical state of terrestrial and oceanic environments (e.g. the distribution of ecosystem production and structure on land and the distribution of nutrients, dissolved oxygen, and marine biota in the oceans); (ii) accounting for paleoclimatic variability in global biogeochemistry and ecology; and (iii) forecasting the responses of ecosystems to climate change and altered anthropogenic nutrient loading (including CO_2), and their feedbacks on global biogeochemistry and climate. Models provide an efficient means to integrate and test our knowledge, especially at large spatial scales.

Contemporary concerns regarding global environmental change have provided the motivation for much of the modeling described in this chapter. Understanding controls on plant production across environmental gradients up to the global scale is a prerequisite for the development of capabilities for predicting the impacts of future environmental change on Earth's ecosystems. In addition to the need to predict impacts, the current interest in the contemporary behavior of the global carbon cycle (driven largely by awareness of the potential consequences of rising concentrations of anthropogenic greenhouse gases for global climate) is responsible for a widening interest in global plant production models. However, attribution of observed atmospheric CO_2 concentrations and their variability in space and time is far from straightforward. In particular, it is currently not possible to unequivocally identify the process or processes responsible for the uptake of the major part of the ≈57% of anthropogenic CO_2 emissions that does not remain in the atmosphere on an annual timescale, or explain why the efficiency of these natural carbon sinks appears to have been decreasing since 2000 (Canadell et al., 2007). Photosynthesis is the primary driver of the contemporary global carbon cycle and, therefore, understanding the dynamics of atmospheric CO_2, and hence future climate, requires a detailed understanding of the global distribution of photosynthesis and how it responds to environmental forcings. Clearly respiration is the other key to determining surface-atmosphere CO_2 fluxes, and the reader is referred to Trumbore (2006) and Amthor (2000) for the terrestrial perspective on this complex subject, and to Geider (1992) and Laws et al. (2000b) for a marine perspective on phytoplankton respiration. Recent marine perspectives on community respiration are given by Williams et al. (2004) and Riser and Johnson (2008).

Researchers have approached the challenges of modeling terrestrial and marine photosynthesis separately; we also briefly consider coastal ecosystems.

A. Terrestrial Photosynthesis

Most models of terrestrial vegetation have a photosynthesis-centric approach, treating plant growth as the carbon balance of photosynthesis, respiration, and litter turnover, with ecosystem dynamics resulting from the relative growth (or productivity) of different physiologies and/or individuals. Photosynthesis and radiation algorithms tend to be the most sophisticated and best understood components of these models, partly because of the relative ease of measuring canopy processes and partly because of the almost universal adoption of the leaf-level, mechanistic model of photosynthesis developed by Graham Farquhar, Susanne von Caemmerer, and Joseph

Berry almost 30 years ago (Farquhar et al., 1980; Chapter 9 of this book by Susanne von Caemmerer, Graham Farquhar and Joseph Berry).

Global-scale models of terrestrial photosynthesis are now an important component of global climate models (GCMs) because of the importance of vegetation processes for soil moisture dynamics and the partitioning of surface energy, processes increasingly shown to be important for the physical climate system (Pitman, 2003). Stomatal conductance algorithms in GCMs are usually based on a representation of photosynthesis (e.g. Randall et al., 1996; Friend and Kiang, 2005), and a few GCMs now predict vegetation growth, and hence surface characteristics, from carbon balance (e.g. Betts et al., 1997; Bonan et al., 2003). An increasing number of GCMs also include a treatment of the global carbon cycle, allowing diagnosis of atmospheric CO_2 concentrations from anthropogenic emissions and net natural surface fluxes. This has led to predictions of future feedbacks between climate and atmospheric CO_2 (Fung et al., 2005; Friedlingstein et al., 2006). However, the outcomes of such model experiments depend critically on the modeled responses of photosynthesis and respiration to temperature and rising atmospheric CO_2, processes poorly constrained in current models.

B. Marine Photosynthesis

Models of marine photosynthesis fall into two broad categories. First, bio-optical algorithms calculate net primary production (NPP) from satellite remote sensing observations of ocean color, sea surface temperature, and solar radiation incident upon the sea surface (Behrenfeld et al., 1997a, b; Carr et al., 2006). These algorithms are used to document the seasonal, interannual, and spatial variability of NPP in the ocean (Behrenfeld et al., 2006; Polovina et al., 2008). Second, dynamic models of plankton ecology and ocean biogeochemistry simulate the present state of the ocean carbon cycle by embedding descriptions of chemical, biogeochemical, and ecological processes within an ocean general circulation model (Doney et al., 2003). These models are used to assess the effects of changes in external forcing on ocean ecosystems and the ocean carbon cycle (Orr et al., 2005; Moore et al., 2006a), to simulate the evolution of the ocean carbon cycle on glacial/interglacial time scales, and to project the ocean carbon cycle into the future (Le Quéré et al.,2005; Schmittner et al., 2008). Accuracy in hindcasting the carbon cycle into the past and forecasting the carbon cycle into the future relies on accurate descriptions of ocean physics, chemistry, ecology, and biogeochemistry (Doney et al., 2003). Primary productivity estimates obtained from these two approaches are largely independent. One point of intersection between the bio-optical algorithms and biogeochemical models is the surface ocean chlorophyll *a* (Chl *a*) field. Satellite derived Chl *a* can be exploited in different ways in the two approaches. The Chl *a* field is an input to bio-optical calculations, whereas it is used in validating biogeochemical models. In addition, assimilation of the Chl *a* field can be used to improve the output of biogeochemical models (Gregg, 2008).

C. Coastal Photosynthesis

Our discussion of marine photosynthesis in this chapter focuses on the phytoplankton, comprising the drifting microscopic algae and cyanobacteria, which account for about 90 percent of marine NPP (Duarte and Cebrián, 1996; Field et al., 1998). None-the-less, we acknowledge the importance of the coastal zone to NPP and the carbon cycle. The coastal zone receives inputs of organic matter and nutrients from terrestrial sources and exchanges organic matter and nutrients with the ocean (Gattuso et al., 1998). The coastal zone includes estuaries, intertidal habitats, shallow water subtidal vegetated habitats, and coral reefs. These habitats are relatively small in spatial extent (Duarte and Cebrián, 1996; Borge et al., 2005), but include a wide range of distinct plant functional groups such as mangroves, salt marsh grasses, seagrasses, benthic microalgae, macroalgae, and endosymbiotic algae within corals. Estimates that these plants contribute about 10% of global marine NPP are obtained by extrapolation from local studies to the global scale on the basis of estimates of the area occupied by these different habitats (Duarte and Cebrián, 1996; Field et al., 1998). As a consequence, NPP of the subtidal benthic communities is poorly quantified. A step towards improving estimates of the contribution of these communities to NPP on a global

scale was taken by Gattuso et al. (2006), who used SeaWiFS imagery to define the surface area of the sea bed where there is sufficient light to support net community production.

II. Description of Model Approaches

Global-scale models of photosynthesis have to confront three major challenges: characterization of the dependency of CO_2 uptake on forcings, the distribution of capacity (i.e. the amounts of Rubisco and light-harvesting machinery) in space and time, and the environmental forcing itself. A wide range of approaches has been used for all three, depending on the intended application and often the background of the researchers. Approaches to the dependency of terrestrial CO_2 uptake on forcings can be classified as either "top-down" or "bottom-up" (the terms refer to strategies of model development: either from the whole to the parts or from the parts to the whole). Marine bio-optical NPP algorithms are similar to the "top-down" terrestrial models, treating NPP as the product of capacity (e.g. Chl *a* concentration) and Chl *a*-specific photosynthesis, which is related to environmental forcing (Field et al., 1998). However, unlike in terrestrial models, marine photosynthesis is rarely treated separately from growth because of the rapid turnover of the phytoplankton.

A. Terrestrial Models

1. CO_2 Fixation

a. "Top-down" Approaches

The most widely used "top-down" approach to modeling terrestrial photosynthesis has its heritage in the ideas of Monteith (1972), who found a linear relationship between absorbed solar radiation and dry matter production of well-watered herbaceous vegetation. A maximum potential efficiency of conversion of energy in the form of radiation to fixed energy in the form of dry matter is assumed, and then scaled depending on the influence of various environmental factors such as temperature and atmospheric vapor pressure deficit (e.g. Running et al., 2004). This approach assumes a linear relationship between total canopy absorbed radiation and photosynthesis, and so can be used with satellite-based measurements of absorbed solar radiation to estimate the global distribution of photosynthesis (e.g. Prince and Goward, 1995). One such photosynthesis product is derived from the MODIS instrument at 8 day intervals, and has global coverage at 1 km resolution (Zhao et al., 2005).

Light-use efficiency (LUE), or the conversion efficiency between absorbed photosynthetically active radiation (APAR) and plant growth, is often given in units of g C $(\text{MJ APAR})^{-1}$. Canopy LUE is determined by many biological and biophysical factors in addition to the maximum quantum yield of photosynthesis, including maximum light-saturated photosynthetic rates, the fraction of photosynthesis consumed by autotrophic respiration, and the diffuse fraction of irradiance (Monteith, 1972, 1977; Prince, 1991; Potter et al., 1993; Field et al., 1998; Ruimy et al., 1999; Running and Hunt, 1993; Goetz and Prince, 1998; Gower et al., 1999; Choudhury, 2001; Running et al., 2004; Jenkins et al., 2007). The widely used CASA carbon cycle model (Potter et al., 1993; Field et al., 1995, 1998; Randerson et al., 1997, 2005) predicts NPP, or gross primary production (GPP) minus autotrophic respiration, as: $\text{NPP} = \text{LUE} \times \text{APAR}$, where $\text{LUE} = \varepsilon^* \times T \times W$. LUE is modeled in CASA as departing from a theoretical universal optimum (ε^*) due to climatic variations given by stress scalar terms for temperature (T) and moisture (W) (Potter et al., 1993; Lobell et al., 2002). Spatial and temporal variations in APAR are prescribed from surface irradiance and the fraction of incident photosynthetically active radiation (f_{PAR}) absorbed by vegetation, derived from satellite observations (Potter et al., 1993; Field et al., 1998; Ruimy et al., 1999).

The model of Sato et al. (2007) uses a rather more complex "top-down" approach than the standard LUE algorithm. Leaf-level photosynthesis is calculated as a simple saturating function of incident PAR, with an initial slope of 0.05 mol CO_2 $(\text{mol quanta})^{-1}$ for C_3 plants. This initial slope is assumed to vary with air temperature and intercellular CO_2 concentration in C_3 leaves, and leaf-level photosynthesis is integrated across 10 cm deep layers within individual tree crowns. Kaduk and Heimann (1996) employ a

similar method to calculate daily canopy light-dependent photosynthesis, but include a canopy-depth dependency for the leaf-level maximum rate and apply linear empirical functions of mean daily temperature, drought stress, and atmospheric CO_2 to the canopy rate; they assume an LUE of 0.07 mol CO_2 (mol quanta)$^{-1}$.

The "TEM" model (Xiao et al.,1998) also uses a "top-down" approach to modeling photosynthesis. Monthly GPP at a given location is calculated as a multiplicative function of responses to incident PAR, leaf area, temperature, atmospheric CO_2, water availability, and nitrogen availability.

b. "Bottom-up" Approaches

C_3 Photosynthesis

"Bottom-up" approaches to modeling environmental regulation of C_3 terrestrial photosynthesis in global models are usually based on the biochemical approach of Farquhar et al. (1980). Instantaneous leaf-level photosynthesis is calculated as the net rate of Rubisco-catalyzed RuBP carboxylation. For a given mean intercellular CO_2 concentration, net carboxylation in all leaf chloroplasts is assumed to be limited either by the Rubisco content and its turnover rate or by the rate of production of RuBP. The latter is limited either by the amount of light absorbed or by the potential rate of electron transport. At high rates of photosynthesis, triose phosphate utilization is sometimes assumed to become limiting (Sharkey, 1985; Harley et al., 1992).

Farquhar et al. (1980) concluded that despite the mechanistic principles of their model, its application requires empirical specification of key parameters. These include Rubisco carboxylase capacity, electron transport capacity, and their respective temperature responses. The situation is challenging as the parameters specifying photosynthetic capacity vary by two orders of magnitude among different species and growth conditions (Wullschleger, 1993). In response, parameter estimation techniques have been developed that utilize observations such as ecosystem CO_2 fluxes measured with the eddy-covariance technique (Knorr and Kattge, 2005; Friend et al., 2007; Wang et al., 2007).

A further concern is that insight gained from the Farquhar et al. (1980) model can be compromised by empirical treatments of the interaction between limiting processes (Rubisco and electron transport) and regulation of electron transport by absorbed light (Badeck, 1995; Kull and Kruijt, 1998). These problems can be overcome by an explicit treatment of the light gradient within leaves. Such an approach not only obviates the need for these empirical functions, but also provides a framework for the mechanistic treatment of the relationship between photosynthesis and leaf nitrogen content (Kull and Kruijt, 1998; Friend, 2001; Friend and Kiang, 2005). Details of this methodology are elaborated below in Section III.

C_4 Photosynthesis

The photosynthetic pathway composition (C_3/C_4 fraction) is a fundamental physiological and ecological distinction in tropical and subtropical savannas, as well as many temperate grasslands (e.g. in the North American Great Plains). C_4 plants have higher photosynthetic rates at high temperatures and under high light (Collatz et al., 1992; Long, 1999) and higher water-use efficiency than do comparable C_3 plants (Pearcy and Ehleringer, 1984; Farquhar et al., 1989; Sage and Monson, 1999). The lower nitrogen requirement of C_4 plants (due to reduced Rubisco content and lack of photorespiratory enzymes) results in a higher photosynthetic nitrogen use efficiency, or the ratio of photosynthesis to leaf nitrogen content.

These functional differences can have important implications for biosphere-atmosphere exchanges of carbon, water, and energy. For example, C_4 plants typically partition more net radiation to sensible heat than latent heat compared to comparable C_3 plants operating under identical conditions. This partitioning has important implications for surface temperature and humidity at regional scales (Sellers et al., 1992).

A hallmark of C_4 plants is their dominance in high light and high temperature grassland and savanna environments (Long, 1999; Sage et al., 1999). The C_4 pathway concentrates CO_2 around the Rubisco enzyme, effectively eliminating the wasteful process of photorespiration, but at the expense of additional energy. This expense

is less critical when solar radiation is abundant, which also raises leaf temperatures and photorespiration in C_3 plants. As a result, photosynthesis in unstressed C_4 leaves does not saturate at high light, unlike the characteristic saturation for most C_3 plants (Collatz et al., 1991, 1992). Canopy models show that under identical conditions C_3 plants are often light saturated while C_4 plants remain light limited under almost all light levels and temperatures (C.J. Still, unpublished). This is supported by eddy flux studies that have examined canopy light responses for different ecosystems (Ruimy et al., 1995; Waring et al., 1995; Gu et al., 2002; Turner et al., 2003; Schwalm et al., 2006; Jenkins et al., 2007). For example, Turner et al. (2003) studied the relationship between gross primary production (GPP) and APAR in a cross-biome comparison. The C_4-dominated tallgrass prairie displayed a nearly linear relationship between GPP and APAR, unlike other biomes that exhibited more typical light saturation (i.e., a hyperbolic relationship between these variables).

C_4 plants will likely respond quite differently than C_3 plants to the suite of anthropogenic global changes being imposed on the Earth system, and this will strongly influence C_3/C_4 distributions and carbon fluxes. In addition to the well-known differences imposed by rising atmospheric CO_2 on photosynthesis (Poorter, 1993; Wand et al., 1999; Morgan et al., 2007), warmer temperatures favor C_4 grasses, while higher CO_2 favors C_3 grasses (Collatz et al., 1998). Changes in the timing of precipitation will be also important, with more cool-season rain typically favoring C_3 grasses and more warm-season rain favoring C_4 grasses. Also, C_3 and C_4 grasses exhibit different responses to nitrogen, with deposition generally favoring C_3 grasses (Wedin and Tilman, 1996a,b; Collins et al., 1998; Brown, 1999). Because of these differences, it is essential to capture spatial and temporal variations in photosynthetic pathway when modeling global photosynthesis and its responses to environmental forcings.

The C_3 photosynthesis model of Farquhar et al. (1980) has been adapted for C_4 physiology by Collatz et al. (1992), who simplified the biochemical-intercellular transport model of Berry and Farquhar (1978) to capture the CO_2 concentration mechanism of C_4 plants. In this model, carboxylation is limited by either light, CO_2 concentration in the mesophyll cells, or Rubisco catalytic activity. Most mechanistic treatments of C_4 photosynthesis in global models utilize this approach (e.g. Sellers et al., 1996a).

2. Photosynthetic Capacity

It is helpful to separate local terrestrial photosynthetic capacity into two components, foliage area and the amount of photosynthetic machinery per unit foliage area. Foliage area is usually quantified as a "leaf area index" (LAI). LAI is the mean, one-sided foliage area per unit ground area, and in global models is typically followed for each vegetation type within each land surface pixel. Models without dynamic nutrient cycles prescribe photosynthetic capacity per unit foliage area from a look-up table of values per biome or vegetation type (e.g. Sellers et al., 1996b; White et al., 2000), or assume unlimited N supply and optimal distribution of N over foliage layers (e.g. the "LPJ" model of Sitch et al., 2003). Foliage area can be prescribed from satellite measurements (Randerson et al., 1997), modeled prognostically (Friend and White, 2000; Sitch et al., 2003; Krinner et al., 2005), or constrained by assimilating measurements into a prognostic model (Demarty et al., 2007).

Global satellite measurements of LAI at 4 km resolution have been derived from the AVHRR sensor, flying on the NOAA series of polar-orbiting satellites since 1978. This instrument was designed purely for operational meteorological applications, but two of the bands have found increasing use since the early 1980s for monitoring vegetation type and condition (Tucker et al., 1985). These two bands are in the visible and near infrared (NIR) frequencies, with green leaves having a higher reflectance of NIR wavelengths and strong absorption of red light by chlorophyll. A normalized difference vegetation index (NDVI) is derived as the ratio of the difference between the measured NIR and visible reflectances and their sum. This index increases with LAI and much work has been undertaken to determine its relationship with vegetation state (Justice et al., 1985; Myneni et al., 1997) and rates of photosynthesis (Nemani et al., 2003; Slayback et al., 2003).

More recently, instruments have been launched into space specifically to monitor terrestrial

vegetation activity. The resulting data are used to calculate indices similar to NDVI, but additional wavebands have been included to enable estimates of the effects of atmospheric properties on individual measurements. A number of these products are now available (Morisette et al., 2006), with the most widely used coming from NASA's Moderate Resolution Imaging Spectroradiometer (MODIS) instrument, which has been used to produce a global 1 km LAI product every 8 days since early 2000 (http://cliveg.bu.edu/modismisr/laifpar/laifpar.html).

Despite their many advantages, all global satellite-based measurements of LAI suffer from problems of saturation and contamination. Particular problems therefore occur in monitoring moist tropical ecosystems. Problems are also evident where changes in background reflectivity contaminate the measurements, such as snow cover. For all these reasons, and for prediction of vegetation activity in the more distant past and in the future, it is essential to develop mechanistic predictive capabilities for LAI. In this role, satellite-based measurements function for model parameterization and validation. However, our current understanding of the complex environmental and biological controls on leaf area display across different species and vegetation types has not allowed the development of a general model of vegetation growth dynamics. LAI has been predicted using fixed C allocation coefficients (Potter et al., 1993; Kucharik et al., 2000), dynamic C allocation and turnover in response to cold and stress factors (Dickinson et al., 1998), and prescribed allometric relationships (Sitch et al., 2003). Other approaches use optimality criteria, such as maximizing NPP with respect to light and soil water (Woodward et al., 1995; Kaduk and Heimann, 1996), maximizing LAI given soil moisture constraints (Neilson, 1995), or assuming a functional balance between access to light, water, CO_2, and soil nutrients (e.g. Friedlingstein et al., 1999). Semi-mechanistic approaches have also been developed, such as following the annual C balance of leaves at the base of the crown (Friend et al., 1997).

All of these methods, to a greater or lesser extent, do well in predicting global relationships among the distribution of mean and maximum LAI and major drivers such as soil moisture and temperature. However, it is unclear if these parameterizations will also hold in the future, when increasing atmospheric CO_2 and changed nutrient relations will interact strongly with climate, hydrological, and species changes and so likely have significant impacts on foliage area and activity. Improved predictive ability for global models will come from knowledge concerning the physiology of allocation in individual plants, followed by calibration using high quality *in situ* and satellite data at the scales of interest.

Leaf phenology refers to the science of the annual cycle of leaf area display. Both the spatial pattern of mean behavior and local inter-annual variability are key components of terrestrial ecosystem models. Timing of leaf display has been the subject of rather more analysis than absolute values of LAI, particularly in temperate forests. However, modeling vegetation-specific phenology at large spatial scales remains a significant challenge (Botta et al., 2000; Kucharik et al., 2006; Kathuroju et al., 2007). Local, species-specific empirical parameterizations of inter-annual variability are well characterized for temperate deciduous forest ecosystems, but their applicability at scales necessary for global simulations is doubtful (Kathuroju et al., 2007). There is clearly a conceptual problem in applying local inter-annual parameterizations to explain mean spatial variability.

Botta et al. (2000) parameterized biome-specific empirical phenological models at the global scale using AVHRR measurements scaled to a 0.5° resolution. Leaf onset is predicted either from a temperature sum (with an influence from the number of chilling days for cool deciduous broadleaf forests) or soil moisture (with a biome-specific time delay from some critical moisture value), depending on the biome type. This approach works well for mean dates in temperature-controlled regions, but is less effective for water-controlled regions such as tropical grasslands and savannas because of greater spatial heterogeneity and data problems. Improvements should result from the development of mechanistic models of grassland growth dynamics.

As mentioned previously, photosynthetic capacity per unit of foliage area in global models of photosynthesis is often prescribed using fixed values for different vegetation types. However, growth conditions can have a large influence

on capacity (Wullschleger, 1993), and so some global models now include an interactive N cycle with prognostic foliage N (Friend and White, 2000; Woodward and Lomas, 2004; Thornton and Zimmerman, 2007). Foliage N is then related to photosynthetic capacity through assumed relationships with Rubisco and chlorophyll concentrations. A problem that remains largely unaddressed, however, is that specific leaf area (SLA), and hence the relationships between LAI, foliage C and N contents, and photosynthetic capacity, is highly variable among species, and even within species under different growth conditions (Knops and Reinhart, 2000). Global models almost all assume a fixed value for each vegetation type, although some recent efforts have been made to make SLA a dynamic variable, at least within canopies (Thornton and Zimmerman, 2007).

Foliage N is thought to limit photosynthesis in many terrestrial ecosystems (Field and Mooney, 1986), although there is evidence that P may be more important than N within the tropics (Vitousek, 1984) due to the highly weathered state and high sorption capacity of many moist tropical forest soils (Lloyd et al., 2001). Although tropical foliar P levels are often limiting, the importance of P for future responses of tropical rainforests to environmental change is unclear given the possibility of desorption of phosphate ions from their fixation sites in response to increased rates of plant uptake (Lloyd et al., 2001). We are not aware of any global photosynthesis/ecosystem model that contains an explicit P cycle (cf. Parton et al., 2005).

It is not clear how best to formulate plant N dynamics in global models. Friend et al. (1997) calculate allocation of N to foliage as a function of total plant N content, with fixed relative C:N ratios among foliage, stem, and fine roots. N is taken up using a function related to the plant N status, fine root mass, and soil mineral N concentration. More sophisticated allocation schemes are being developed in which foliage N dynamics are controlled by the local transpiration rate, as indicated by experimental results (Pons and Bergkotte, 1996), a methodology that has interesting implications for the mechanistic modeling of soil moisture effects on LAI and phenology.

The local foliage N content accounts for only part of the relation between nutrient availability and plant photosynthetic capacity. Experimental evidence indicates that in most species studied, N supply actually has a greater influence on leaf area than on capacity per unit leaf area. For example, Taub (2002) measured a 37% increase in mean leaf mass in response to fertilization across 17 C_3 grass species, whereas mean growth rate per unit leaf area increased by only 12%. Studies such as this demonstrate that allocation shifts in response to nutrient supply need to be carefully included in global models.

3. Environmental Forcing

Global-scale models of terrestrial photosynthesis generally treat the supply of CO_2 to the chloroplasts much more simply than controls on photosynthesis itself. Most approaches explicitly consider stomatal conductance and leaf and/or canopy boundary layer conductance. However, the complexity of stomatal behavior is typically avoided by assuming that stomata act to maintain the intercellular air space concentration of CO_2 (C_i) at some specified ratio to the external concentration (C_a), thereby allowing calculation of stomatal conductance directly from the rate of net photosynthesis (A_n). This ratio is assumed fixed as light, temperature, and CO_2 concentration vary, with different values for C_3 and C_4 leaves. However, changing hydrological factors such as the leaf-to-air humidity gradient and soil moisture content change C_i/C_a, and this dependency can be included. Compelling evidence for the conservative nature of C_i/C_a was provided by Wong et al. (1979). However, a complication for practical applications is that A_n depends on C_i, requiring an iterative modeling process to obtain and equilibrium value of C_i under any given set of forcing conditions.

A frequently used parameterization of leaf-level stomatal conductance (g_{sc}), derived by Ball et al. (1987) from their own observations and subsequently modified by Leuning (1995), is:

$$g_{sc} = g_0 + \frac{a_1 A_n}{(C_S - \Gamma) \cdot \left(1 + \frac{D_S}{D_0}\right)}, \qquad (20.1)$$

where D_s and C_s are the leaf surface vapor pressure deficit and CO_2 concentration, respectively, g_0 is conductance as $A_n \to 0$ when light $\to 0$, Γ is the CO_2 compensation point for

net photosynthesis, D_0 is the value of D_s that reduces $g_{sc} - g_0$ by 50%, and a_1 represents the slope of the relationship between conductance and net photosynthesis. It is well known that stomata close at low soil moisture contents, but it is not clear how this behavior should be combined with Eq. (20.1), resulting in a range of different, albeit simple, approaches. A fundamental issue is whether stomata respond directly to soil moisture, or through changes in photosynthetic capacity, as seems likely after sufficient time for adjustments (Wong et al., 1979). The "SiB2" model of Sellers et al. (1996a) and the Dynamic Global Vegetation Model (DGVM) of Krinner et al. (2005) reduce photosynthetic capacity under soil moisture stress, and then use the Ball et al. (1987) formulation for stomatal conductance, thereby simultaneously reducing photosynthesis and stomatal conductance.

Methodologies for calculation of atmospheric forcing and surface energy and water balances vary greatly depending on the model timestep, whether or not the aim is to explore climate feedbacks, and the general interests of the researchers. Weather generators are frequently employed to introduce daily weather variability given long-term mean-monthly climate (Friend, 1998). Sometimes these are extended to subdaily timesteps. There is great variation in the detail with which the canopy boundary layer is treated, ranging from no explicit treatment (Sitch et al., 2003), to simple treatment of a canopy boundary layer (Woodward and Lomas, 2004), and full coupling to GCMs (Foley et al., 1998; Friend and Kiang, 2005). The level of detail used to treat atmospheric processes tends to be replicated for below-ground hydrology and surface energy balance.

Many global photosynthesis models use the so-called "big-leaf" hypothesis for the scaling of leaf-level photosynthesis (and stomatal conductance) to the canopy, despite significant doubts as its validity (Friend, 2001; Chapter 16 of this book by Ülo Niinemets and Niels P. R. Anten). More realistic approaches consider vertical gradients in photosynthetic capacity and radiation environment, including direct and diffuse irradiance and sun and shade leaves (Bonan et al., 2003). It is perhaps surprising that the radiation environment is frequently modeled in a somewhat *ad hoc* fashion, with little justification given for the level of detail chosen and frequently no use of observations to constrain the approach, particularly with respect to different canopy geometries. Nevertheless, strong evidence exists that correctly simulating the canopy radiation environment is critical for accurate simulation of canopy photosynthesis (Friend, 2001; Baldocchi and Wilson, 2001).

B. Marine Models

1. Photosynthetic Capacity

Primary productivity in the sea is driven by a combination of physical, chemical, and biological factors. The most important is the biomass of phytoplankton, which is analogous to the "photosynthetic capacity" as defined in the previous section on terrestrial photosynthesis. Chlorophyll *a* is the most commonly used index of phytoplankton biomass because it is specific to the phytoplankton, and can be readily measured by a variety of methods on different space and time scales. In addition to spectrophotometric and fluorimetric determinations on samples extracted in polar solvents (Jeffrey et al., 1997), these methods include *in situ* sensing of chlorophyll fluorescence (Falkowski and Kiefer, 1985) and remote sensing of ocean color (O'Reilly et al., 1998; Morel et al., 2007).

Global distributions of chlorophyll concentration are available from several sensors including CZCS in the 1980s, and more recently SeaWiFS, MODIS-Aqua, and MERIS (Antoine et al., 2005; Morel et al., 2007). Chlorophyll *a* concentrations derived using these sensors agree over a wide range (0.1–3 mg m^{-3}), but diverge at the low Chl *a* concentrations (<0.1 mg m^{-3}) characteristic of the oligotrophic open ocean regions (Morel et al., 2007). Satellite estimates compare favorably with surface observations on discrete samples (Gregg and Casey, 2004), especially when issues regarding the validity of these "truth" observations are taken into account (Marrari et al., 2006). However, sampling errors may bias estimates of monthly and annual mean Chl *a* concentrations (Gregg and Casey, 2007b). Overestimates were inferred for regions that are poorly sampled due to low sun angle or high cloud cover (Gregg and Casey, 2007b). These are the times/locations when/where phytoplankton

growth is reduced (and thus Chl *a* concentrations are low) because incident light is low.

Satellite measurements of ocean color provide estimates of Chl *a* concentration for the upper 20% of the euphotic zone. However, the Chl *a* profile often shows vertical structure with a subsurface maximum that lies at depths where photosynthesis is limited by light. Surface observations of Chl *a* can be extrapolated to the entire euphotic zone based on typical vertical profiles of Chl *a* obtained from a climatology of *in situ* observations (Sathyendranath et al., 1995), or from empirically derived relationships between surface Chl *a* and the subsurface vertical distributions (Uitz et al., 2006).

The Chl *a* concentration can be reduced when incident light is low and/or nutrients are limiting. The light environment experienced by phytoplankton depends on the vertical attenuation of light and the mixed layer depth (MLD). In the clearest ocean waters, net photosynthesis can occur to depths of about 150 m. However, as Chl *a* concentration increases, light penetration decreases (Morel and Maritorena, 2001). At a concentration of 1 mg Chl $a\,m^{-3}$, the photic zone depth declines to about 25 m, whereas at $10\,mg\,m^{-3}$ Chl *a*, the photic zone is only about 10 m deep (Morel and Maritorena, 2001).

The MLD can vary from about 10 to >500 m. Phytoplankton are redistributed within the mixed layer by turbulence on time scales <1 day. During seasons when incident solar radiation is low and the surface layer is deeply mixed, light limits marine photosynthesis. At mid- and high-latitudes in winter the Chl *a* concentration typically drops to about $0.1\,mg\ m^{-3}$ (Ward and Waniek, 2007). In temperate and polar regions during winter, the combination of low Chl *a* and low incident light limit primary production. Light limitation may be exacerbated by low Fe availability leading to Fe-light co-limitation (Boyd et al., 2001). During spring, Chl *a* concentration increases as incident solar radiation increases and the mixed layer shoals, consistent with critical depth theory (Follows and Dutkiewicz, 2001).

In the tropics, and in temperate latitudes during summer, the mixed layer typically lies within the euphotic zone and inorganic nutrients are limiting. In these oligotrophic waters, Chl *a* concentration drops below $0.1\,mg\,m^{-3}$. Nutrient limitation can be described either in terms of Liebig-type limitation of yield (e.g. of Chl *a* concentration) or Blackman-type limitation of growth rate (Cullen et al., 1992). Both types of limitation operate in the sea. Liebig-type limitation may impose a greater constraint on primary productivity because, at a given incident photon flux density, primary productivity is proportional to phytoplankton biomass, and Liebig-type nutrient availability sets an upper limit to biomass. Blackman-type limitation of growth rate may be superimposed on Liebig-type limitation of biomass to further reduce primary productivity. For example, the upper limit on phytoplankton biomass may be set by the N upwelled from deep waters, but CO_2 and/or Fe may limit the rate at which inorganic N is converted into biomass (Moore et al., 2006b), and/or affect the composition of the phytoplankton assemblage (Tortell et al., 2002). Finally, co-limitation may act in several ways to limit the growth rate and/or affect the community structure of the phytoplankton (Arrigo, 2005).

2. Bio-optical Algorithms

An index of the light utilization efficiency, widely used in marine systems, is defined in Eq. (20.2). This efficiency, designated Ψ, is obtained by dividing the time- and depth-integrated primary productivity by the product of the depth-integrated Chl *a* concentration and the time-integrated photon flux incident upon the sea surface (Falkowski and Raven, 2007):

$$\Psi = \frac{\int_{\text{dawn}}^{\text{dusk}} \int_0^{Z_C} \text{NPP}\,(z,t)\,dz dt}{\int_0^{Z_C} Chl\,(z)\,dz \cdot \int_{\text{dawn}}^{\text{dusk}} E_0 dt}. \qquad (20.2)$$

In this equation, NPP(z, t) is the net carbon fixation rate, $Chl(z)$ is the Chl *a* concentration, and E_0 is the incident PAR. The integration in time (t) is from dawn to dusk, and the integration over depth (designated z) is from the surface ($z = 0$) to the bottom of the euphotic zone ($z = z_c$). Ψ can be considered to be the product of the water-column-averaged optical cross-section and the water-column-averaged quantum efficiency of photosynthesis (Falkowski and Raven, 2007). Where the value of Ψ is known, Eq. (20.2) can be rearranged to calculate the daily water column integral NPP from the Chl *a* concentration and the incident PAR. Based on a review of the

data available at the time, Platt (1986) suggested that Ψ varied by about $\pm 40\%$ around a typical value of 0.48 g C (mol photons)$^{-1}$ m^2 (g Chl a)$^{-1}$. More recently, based on more comprehensive coverage of the global ocean, Falkowski and Raven (2007) showed that Ψ varies much more widely (from <0.1–1.5).

To obtain more accurate estimates of marine primary production, oceanographers employ bio-optical remote sensing algorithms. These algorithms can be classified into four categories depending on the whether the algorithm resolves the depth, time, and/or wavelength dependencies of photosynthetic rate (Behrenfeld and Falkowski, 1997b). Central to bio-optical algorithms is treatment of NPP as the product of the Chl a concentration $Chl(z,t)$, g m^{-3}, and the Chl a-specific net photosynthesis rate P^{Chl}, g C (g Chl a)$^{-1}$ h^{-1}:

$$\mathrm{NPP}(z,t) = Chl(z,t) \cdot P^{\mathrm{Chl}}(z,t). \quad (20.3)$$

There are two basic approaches to parameterizing the light dependence of P^{Chl} (Sathyendranath and Platt, 2007). First, P^{Chl} can be specified as a function of PAR (Sathyendranath and Platt, 1989). In this case, the photosynthesis light curve is parameterized in terms of the light-saturated photosynthesis rate and the light-limited initial slope. These models are often resolved spectrally because the initial slope scales with the Chl a-specific light absorption coefficient, which varies with wavelength. A third parameter may be employed to describe the inhibition of photosynthesis at supraoptimal PAR. In the second approach, primary productivity is calculated from the product of the rate of light absorption and the quantum efficiency of photosynthesis (Morel, 1991). In this case, both the maximum quantum efficiency and the dependence of quantum efficiency on the rate of light absorption are specified. Provided that compatible mathematical formulations are chosen for the photosynthesis versus PAR and quantum yield versus PAR curves, these approaches are equivalent (Geider, 1990; Morel et al., 1996; Sathyendranath and Platt, 2007).

The coupling of photosynthesis to light and the effects of phytoplankton on the attenuation of light in water vary markedly with the wavelength of PAR. Phytoplankton dominate the variable component of light attenuation in open ocean waters where the concentrations of colored dissolved organic matter and suspended particulate matter are low (Morel and Maritorena, 2001). Phytoplankton cells absorb a variable proportion (typically <10–70%) of the incident photons (Stramski and Mobley, 1997), and variations in cell size and cellular Chl a content lead to systematic variations in the Chl a-specific light absorption coefficient (Bricaud et al., 2004; 2007). In addition, the composition of photosynthetic pigments varies widely, and this variability affects the shape of the light absorption spectrum and thus NPP in the light-limited regions of the photosynthesis-PAR response curve (Sathyendranath and Platt, 2007). This spectral variability may affect competition for light in nature (Wood, 1985; Stomp et al., 2007). These are compelling reasons for including spectral dependencies in bio-optical algorithms (Morel et al., 1996; Behrenfeld, 1997b; Smyth et al., 2005; Sathyendranath and Platt, 2007).

The effects of temperature, photoacclimation, and nutrient limitation can be introduced by specifying how these variables affect the parameters of the photosynthesis-PAR relationships. For example, the light-saturated rate increases with temperature and declines in response to nutrient limitation or light limitation. Although sea surface temperature can be estimated directly using satellite remote sensing, the effects of these limitations must be obtained indirectly. Nutrient concentrations (N, P, Si) can be inferred from their correlation with temperature, although such correlations are site specific (Kamykowski et al., 2002; Switzer et al., 2003). The effect of light limitation can be parameterized in terms of the optical depth and incident PAR. Although we have a general understanding of how phytoplankton photosynthesis responds to these environmental variables based on laboratory studies (Geider et al., 1998), it is difficult to use this information directly in bio-optical algorithms. Instead, we rely on empirical relationships developed using ship-based observations. Perhaps the biggest obstacle to accounting for the effects of environmental variables on the parameters of the photosynthesis-PAR relationship is undersampling in the world ocean (Banse and Postel, 2003; Carr et al., 2006).

There have been several round-robin comparisons of the performance of bio-optical algorithms of pelagic primary productivity. The most recent of these (Carr et al., 2006) found that global estimates of annual marine primary productivity varied by a factor of two amongst the 24 bio-optical models examined. A common set of input data consisted of sea surface Chl *a* concentrations, sea surface temperature, incident PAR, and MLD. The algorithms varied in complexity. The simplest algorithm estimated NPP directly from Chl *a* concentration without considering any of the other input variables. The most complicated algorithms included depth resolution of Chl *a* concentration and spectral resolution of PAR. The major limitations in the application of bio-optical algorithms identified were gaps in the observations of phytoplankton photosynthesis across the full range of conditions encountered in the ocean (Carr et al., 2006).

The Chl *a*-specific net photosynthesis rate (P^{Chl}), although commonly reported by oceanographers (MacIntyre et al., 2002) and commonly employed in bio-optical algorithms, is a poor index of phytoplankton growth. This is because there is taxonomic and phenotypic plasticity in the ratio of Chl *a*-to-biomass (Geider et al., 1998; Behrenfeld et al., 2005). For many applications, the carbon-specific rate of photosynthesis is more informative. Carbon-specific photosynthesis has units of inverse time and can be related to the specific growth rate (μ with units h^{-1}), provided that growth and net photosynthesis are measured on the same time scale. μ is related to P^{Chl} (with units of g C (g Chl a)$^{-1}$ h^{-1}) as follows:

$$\mu = \theta \cdot P^{\mathrm{Chl}}, \tag{20.4}$$

where θ is the Chl *a*-to-carbon ratio in g Chl *a* (g C)$^{-1}$.

Recently, bio-optical algorithms have been developed to estimate carbon-specific photosynthesis from satellite data (Behrenfeld et al., 2005; Westberry et al., 2008). These models also provide estimates of the carbon-to-Chl *a* ratio of the phytoplankton, which can be used as an index of the degree of light acclimation and nutrient limitation. This approach predicted a similar global marine NPP to other bio-optical approaches. However, the distributions of NPP in space and time differed significantly between the Chl *a*-based and carbon-based algorithms (Westberry et al., 2008). This approach is used to obtain a new estimate of marine primary production in Section III.B.

Most bio-optical algorithms calculate NPP as the product of a capacity (e.g. the Chl *a* concentration) and a "conversion efficiency" (e.g. P^{Chl}), as in Eq. (20.3). However, it is not necessary to explicitly separate "capacity" from "conversion efficiency", because NPP can be expressed as:

$$\mathrm{NPP}(z,t) = f\left[Chl(z,t), N(z), T(z), E(z), \ldots\right], \tag{20.5}$$

where z is the depth, $N(z)$ is the concentration of a limiting nutrient "N" at depth z, $T(z)$ the temperature at depth z, $E(z)$ is the photon flux density at depth z, etc. (Huot et al., 2007). In Eq. (20.5), remotely sensed Chl *a* serves directly as a predictor of NPP, together with other variables inferred from satellite remote sensing and/or climatologies (Huot et al., 2007). One can take this approach a step further by employing a biomass-independent algorithm that uses estimates of inherent optical properties rather than Chl *a* in the calculation of NPP (Sathyendranath and Platt, 2007).

Processes other than photosynthesis are important in determining marine NPP and the role of marine ecosystems in the carbon cycle. These processes include export production, calcification, and nitrogen fixation.

On land, atmospheric carbon in CO_2 can be sequestered in biomass and/or soil organic matter. These two compartments are in intimate contact with the atmosphere. In the oceans, phytoplankton sequester atmospheric carbon by facilitating its transport to the deep ocean, thus removing it from intimate contact with the atmosphere. This biologically driven vertical transport of carbon is referred to as the "biological pump" (Sigman and Haug, 2003). The biological pump consists of uptake of CO_2 and nutrients by phytoplankton near the sea surface (typically <150 m deep), sinking of particulate organic matter to below the permanent thermocline ($>1{,}000$ m deep), and remineralisation of organic matter to CO_2 and nutrients in the deep ocean or burial of organic carbon in the sediments (Sigman and Haug, 2003). Primary production removed from

the surface water by the biological pump is referred to as export production. Export production can be calculated from bio-optical algorithms of NPP by including further parameterizations describing the relationship between NPP and particle sinking (Dunne et al., 2007), which may be related to food-web structure (Laws et al., 2000a). For the ocean as a whole, export production accounts for about 20% of NPP (Laws et al., 2000a; Dunne et al., 2007).

Many marine organisms have calcium carbonate shells or scales. Amongst the important groups of planktonic calcifiers are coccolithophorids, foraminifera, and pteropods. Calcification removes inorganic carbon from the ocean, but increases the partial pressure of CO_2 (p_{CO2}). This is evident from the stoichiometric equation for the precipitation of calcium carbonate: $Ca^{2+} + 2\ HCO_3^- \leftrightarrow CaCO_3 + CO_2 + 2H^+$. This increase of p_{CO2} due to calcification partially offsets the ability of the ocean biota to sequester atmospheric CO_2 by the biological pump. However, $CaCO_3$ acts as ballast, which accelerates the sinking of organic matter, potentially increasing export production. Recently, algorithms for the remote sensing of suspended calcium carbonate concentration (Balch et al., 2005) and the rate of calcification (Balch et al., 2007) have been developed and applied.

Nitrogen fixation provides up to 50% of the key limiting resource of fixed nitrogen in large parts of the oligotrophic open ocean. This new nitrogen allows increased phytoplankton biomass and primary productivity. Blooms of the colonial diazotroph *Trichodesmium* appear to be superimposed on a low background rate of N_2 fixation. These blooms are considered to make a major contribution to oceanic N_2fixation (Capone et al., 2005). Recently, algorithms for detecting *Trichodesmium* blooms from water-leaving radiance have been developed (Westberry and Siegel, 2006). The spatial patterns of *Trichodesmium* blooms retrieved by these algorithms are largely consistent with previously reported blooms (Westberry and Siegel, 2006), with putative *Trichodesmium* blooms found most often in the eastern tropical Pacific and the Arabian Sea. The nitrogen cycle is closely coupled to the carbon cycle in marine systems, and increased understanding of the sources and sinks of fixed nitrogen (Deutsch et al., 2007; Duce et al., 2008) will continue to inform models of marine NPP and export production.

3. Biogeochemical Models

Whereas the NPP of phytoplankton can be obtained from bio-optical algorithms, investigations of the response of the marine carbon cycle to climate change employ biogeochemical models. Biogeochemical models examine the coupling of plankton dynamics to ocean physics. Unlike terrestrial vegetation, which is rooted in place, the oceans are a dynamic fluid. Phytoplankton are suspended in the water column and drift with the currents. The nutrients that phytoplankton need to grow and the grazers that feed on the phytoplankton also drift with the currents. To account for these effects, models of ocean ecosystems are embedded within physical models of ocean circulation and mixing (e.g. Ocean General Circulation Models). At any point in the ocean, the rate of change of phytoplankton biomass is determined by the physical processes of advection and diffusion, and the ecological processes of production (e.g. photosynthesis and nutrient uptake), consumption (e.g. grazing), and dissipation (e.g. respiration and excretion) (Doney et al., 2003).

Current models of plankton ecology and biogeochemistry can be traced to the seminal work of Fasham et al. (1990). These authors embedded an ecological model, which represented the state-of-the-art understanding of plankton processes in the late 1980s, within a simple physical model of the annual cycle of incident solar radiation, MLD, vertical exchange, and vertical nutrient fluxes at one location in the Sargasso Sea near Bermuda. Inorganic nitrogen and light were the only limiting factors in the ecological model. The model included two inorganic forms of nitrogen (nitrate and ammonium) and five ecological components (phytoplankton, zooplankton, bacterioplankton, dissolved organic nitrogen, and detritus). Models derived from Fasham et al. (1990) are sometimes referred to as NPZD models, indicating that they describe the dynamics of inorganic Nutrients, Phytoplankton, Zooplankton, and Detritus. NPZD models have been embedded within 3D ocean GCMs to study ocean plankton dynamics

and plankton biogeochemistry at the basin scale (Sarmiento et al., 1993) and ocean scale (Popova et al., 2006a, b).

NPZD models were developed to examine the effects of changes in physical forcing (primarily seasonal variability of MLD) on seasonal and spatial variability of chlorophyll concentration (Fasham et al., 1990). These models lack taxonomic resolution, and Chl *a* is used to represent the biomass of all phytoplankton groups. More recently, dynamic green ocean models (DGOMs) have been developed to study the feedbacks between climate and the ocean microbiota (Le Quéré et al., 2005; Hood et al., 2006; Gregg and Casey, 2007a). The most sophisticated of these DGOMs include several phytoplankton functional groups and several interacting element cycles. Typically, two of the functional groups are defined taxonomically, namely the diatoms and the diazotrophs (which use N_2 as a nitrogen source), and two of the functional groups are defined by cell size, namely the picophytoplankton (0.2–2 μm nominal diameter) and nanophytoplankton (2–20 μm diameter). DGOMs may also include calcifying organisms (coccolithophorids and foraminifera in the open ocean) as functional groups because of the importance of calcification in the marine carbon cycle (Orr et al., 2005). The element cycles included in the models are those of C, N, P, Fe, and Si. Of these five elements, N, P, Fe, or Si can limit phytoplankton growth rate and yield.

The model of Moore et al. (2004) illustrates the importance of including different functional groups in models of upper ocean biogeochemistry. Diazotrophs accounted for about 0.5% of primary production, but fixed enough N_2 to provide the N source that supported about 10% of primary production and 8% of export production (Moore et al., 2004). In this work, diatoms disproportionately contributed to export production, but $CaCO_3$ from the coccolithophores was the key driver of the export flux to the deep ocean. Unfortunately, different DGOMs may yield widely different assessments of the contributions of key functional groups, including diatoms and coccolithophores, to NPP (Gregg and Casey, 2007a), indicating that a consensus model has yet to be achieved.

4. Environmental Forcing

Models of ocean biogeochemistry typically divide the ocean into a set of vertical divisions within a latitude/longitude grid (Doney et al., 2003). The output of the biogeochemical models is affected by the sizes of the boxes in the grid and the physical oceanographic model within which the biogeochemical model is embedded (Berline et al., 2007). The spatial resolution of the physical model, both in the vertical and in the horizontal, affects the fidelity of the physical model in representing ocean circulation and mixing. The fidelity of the physical model is also affected by temporal resolution, especially with respect to the ability of the model to represent vertical mixing near the sea surface. Errors in the physical model will lead to errors in nutrient fluxes and the light environment, and thus affect the output of the biogeochemical model (Berline et al., 2007; Najjar et al., 2007).

A recurrent problem in plankton biogeochemical models is underestimation of primary productivity in the oligotrophic subtropical gyres relative to observations (McGillicuddy et al., 1998; Berline et al., 2007). The problem applies not only to NPP in models, but also to accounting for export production (McGillicuddy et al., 1998). Although underestimation of the rate of nitrogen fixation may account for some of the discrepancy, it is also clear that inclusion of mesoscale processes, which were neglected in course resolution ($>2°$) models, is necessary to obtain accurate nutrient budgets.

Mesoscale eddies (50–100 km diameter) play an important role in transporting heat, salinity, momentum, and nutrients in the ocean. Mesoscale eddies increase nutrient supply and thus primary production in the nutrient-impoverished subtropical ocean (McGillicuddy et al., 1998, 2007). If the perturbation in nutrient supply is sufficient to change the structure of the open ocean food web, then the operation of the biological pump may also be affected (Laws et al., 2000a; Brix et al., 2006). Associated with eddies are sub-mesoscale (5–10 km wide) features. Nutrient transport associated with these features may be as important as that attributed to the mesoscale eddies (Lapeyre and Klein, 2006;

McGillicuddy et al., 2007). With increases in computing power, the latitudinal and longitudinal resolution of GCMs has increased from $>2°$ to $<0.1°$ (McGillicuddy et al., 2003), providing enough spatial resolution to represent important mesoscale oceanographic features.

Vertical mixing and stratification have long been known to play significant roles in plankton ecology and ocean biogeochemistry (Platt et al., 2003; Popova et al., 2006b). MLD is affected by seasonal periodicity (e.g. solar radiation and wind patterns), long-term fluctuations in the climate system (e.g. ENSO and other teleconnections), episodic events (e.g. storms), and the diel cycle of solar radiation. MLD in turn affects the entrainment of nutrients from deep waters to the photic zone, the detrainment of organisms and organic matter from the photic zone to the deep ocean, and the light environment encountered by phytoplankton (Platt et al., 2003). Phytoplankton biomass and productivity respond primarily to variability in mixing and nutrient fluxes, and survival of zooplankton through the winter also depends on the extent of mixing (Popova et al., 2006b).

Most biogeochemical models used to describe the current state of the ocean employ a time step of one day, whereas models designed to examine the evolution of the ocean carbon cycle on time scales of 100–1,000 years employ longer time steps, typically a month. In a recent study, Popova et al. (2006b) examined how the time step, which ranged from 6 h to 1 month, affected the simulation of NPP and new production in a global ocean biogeochemical model. Diel variability of MLD (Woods and Onken, 1982) appeared to be particularly important in controlling the performance of the biogeochemical model (Popova et al., 2006b). The mixed layer shoals during the day as solar radiation heats the surface waters, trapping plankton near the surface. MLD increases at night as loss of heat from the sea surface leads to convective mixing, redistributing the plankton into deeper waters and transporting nutrients to the surface.

Physical forcing refers not only to ocean circulation and MLD, which are affected by incident solar radiation, but also to the input of nutrients to the sea surface. Inorganic and organic nitrogen, phosphorus, and trace elements are deposited to the surface ocean in wet and dry deposition from the atmosphere (Jickells et al., 2005; Duce et al., 2008). In particular, with the recognition that Fe is a limiting nutrient for NPP in about 1/3 of the ocean, designated as High-Nitrate/Low-Chlorophyll (HNLC) regions (de Baar et al., 2005), and that Fe may limit N_2 fixation in oligotrophic ocean regions that account for most of the rest of ocean surface area (Falkowski, 1997), the deposition of Fe-containing aerosols has been recognized to play an important role in ocean carbon cycle (Moore et al., 2006b; Moore and Doney, 2007). The aeolian supply of nutrients can be specified from dust deposition fields derived from atmospheric transport models such as GOCART (Ginoux et al., 2001), and assumptions regarding the N, P, and Fe content and solubility in the atmospheric aerosols.

III. Global Simulation

A simulation is presented here to illustrate the state-of-the-art of modeling photosynthesis at the global scale. Mean annual terrestrial and marine fields of the recent historical period are combined to give a global picture. The first such combined assessment was published by Field et al. (1998); the simulation presented here is designed to be an update to this. The terrestrial simulation uses the mechanistic biochemical model described by Friend and Kiang (2005), with some modifications, and the marine simulation uses the bio-optic "Carbon-based Primary Model" (CbPM) model of Westberry et al. (2008).

A. Terrestrial Photosynthesis

1. CO_2 Fixation

Foliage-level C_3 photosynthesis is modeled using the approach of Kull and Kruijt (1998) as implemented by Friend (2001) and Friend and Kiang (2005), but with some improvements (e.g. improved handling of numerical roots when solving for the intercellular air space CO_2 concentration). Kull and Kruijt (1998) took as their starting point the model of Farquhar et al. (1980) and added a treatment of light extinction over chloroplasts to separate regions of the leaf that are light-saturated or light-limited. Photosynthesis in

the light-saturated region is taken as the minimum of the electron transport capacity- and Rubisco-limited rates. Under many conditions, light extinction over the light-saturated chloroplasts causes the rate of CO_2 fixation in deeper chloroplasts to be limited by the rate of light harvesting. Photosynthesis in this region is a linear function of the total amount of light absorbed by light-limited chloroplasts and the intrinsic quantum efficiency. All three rates are expressed on an N basis, enabling straightforward scaling to the leaf and canopy levels. Kull and Kruijt (1998) showed that if the chlorophyll to N ratio is assumed constant throughout the leaf, then the following analytical solution can be derived:

$$A = \left(1 - \frac{\Gamma^*}{C_\mathrm{i}}\right) \cdot \left[m_\mathrm{sat} N_\mathrm{sat} + \alpha m_1 I_\mathrm{a}\right], \quad (20.6)$$

where A is total leaf photosynthesis, Γ^* is the CO_2 partial pressure for the compensation of oxygenation and carboxylation reactions, C_i is the partial pressure of CO_2 in the intercellular air space, m_sat is the N-normalized rate of light-saturated carboxylation (i.e., the minimum of the electron transport capacity- and Rubisco-limited rates), N_sat is the cumulative N at which limitation by light harvesting occurs, α is the intrinsic quantum efficiency, m_1 is the ratio of the CO_2-controlled RuBP supply-limited carboxylation rate to its theoretical maximum, and I_a is the amount of light absorbed by light harvesting-limited chloroplasts. A single extinction coefficient is used to calculate light absorption over chloroplasts, and N_sat is calculated from m_sat, total leaf N, and total absorbed light.

This approach has been shown to perform substantially better than the traditional implementation of the Farquhar et al. (1980) model for a wide range of forest canopies (S. Zaehle and A.D. Friend, unpublished).

The approach of Kull and Kruijt (1998) was adapted for C_4 physiology, with the same overall approach of separation of light-saturated and light-limited regions. However, bundle-sheath chloroplast CO_2 is assumed to be 7,800 Pa – as calculated from the full intercellular (ICT) transport model of Collatz et al. (1992) under peak photosynthetic rates – and an additional potential limitation to light-saturated photosynthesis from the CO_2 concentrating mechanism is included. This is parameterized as a linear dependence on the CO_2 concentration in the intercellular spaces of the mesophyll (after Eq. 4A of Collatz et al., 1992), with a $Q_{10} = 2$ temperature dependence and a linear scaling factor relating the PEPcase rate constant for CO_2 to foliar photosynthetic N content (calibrated using the ICT model to be 3.2 mol CO_2 (mol N)$^{-1}$ s^{-1}). In addition, the fractional RuBP quantum requirement for the production of RuBP in the bundle-sheaths is assumed to be 0.6 (Berry and Farquhar, 1978).

2. Photosynthetic Capacity

Terrestrial vegetation is classed into seven generalized plant types (GPTs), and each is assigned typical parameter values related to its foliage physiology (Table 20.1). These values were derived from the literature (see legend to Table 20.1) and *in situ* measurements at representative sites compiled in the FLUXNET database of eddy-covariance CO_2 flux sites (Friend and Kiang, 2005). The natural variation in these parameters between species and growth conditions within each GPT is very wide, particularly for specific leaf area and foliar N content. Nevertheless, the use of typical values addresses the overall broad regional behavior of vegetation for global-scale studies. More local assessments would require greater precision in biological (and physical) parameterization.

Each terrestrial ¼° pixel is assigned a dominant GPT using the Loveland et al. (2000) land cover database with the SiB classification system. This is an AVHRR-based product, and dominant cover types were each assigned to dominant GPTs using the mapping given in Table 20.2.

Mean-monthly LAI is prescribed from observations made by the MODIS instrument and available through the Department of Geography, Boston University (http://cliveg.bu.edu/; Yang et al., 2006). A complication arose from misalignment between the original ¼° dataset (MOD15_BU) and the actual distribution of land area, particularly in Oceania, necessitating adjustments by eye to the original grid. A mean-monthly LAI climatology was then created from the original February 2000–December 2006 data. These data are used to prescribe monthly LAI in the global photosynthesis simulations without temporal interpolation.

Table 20.1. Parameter values assigned to the different generalized plant types (GPTs) used in the global terrestrial simulations. GPT codes are: NLEV = needleleaf evergreen, BREV = broadleaf evergreen, NLCD = needleleaf cold deciduous, BRCD = broadleaf cold deciduous, C3GR = C_3 herbaceous, and C4GR = C_4 grass. Specific leaf areas (*SLA*s) come from Bond-Lamberty and Gower (2007) (moss: mean of min and max measurements); White et al. (2000) (NLEV, NLCD, BRCD, C3GR); McWilliam et al. (1993) (BREV; mean assuming 0.5 kg [C] kg $[DM]^{-1}$); and the value for C4GR is assumed equal to that for C3GR. *N* (foliar N content as percentage of dry mass) taken from Liu et al. (2007) (moss), White et al. (2000) (NLEV, NLCD, BRCD, C3GR), Martínez-Sánchez et al. (2003), assuming SLA used here (BREV), and calibrated against CO_2 flux data from Hanan et al. (2005) (C4GR). f_N is relative photosynthetic capacity per unit foliar N, calibrated from eddy-covariance flux data as described by Friend and Kiang (2005) (NLEV, BREV, BRCD, C3GR); C4GR f_N is calibrated against CO_2 flux data from Hanan et al. (2005); moss f_N is set to the default value in the original Kull and Kruijt (1998) model; NLCD f_N is set to the value for BRCD. Minimum foliar surface conductance to water, g_{min}, is assumed infinite for moss (very thin cuticle); other values come from Vostral et al. (2002) (NLEV, assumed the same for NLCD); and the rest are calibrated from latent heat flux data (Friend and Kiang 2005; Hanan et al., 2005)

GPT	*SLA* m^2 kg $[C]^{-1}$	*N* % [DM]	f_N fraction	g_{min} mm s^{-1}	g_{max} mm s^{-1}
Moss	61	2.6	1	∞	∞
NLEV	8.2	1.1	0.9	0.04	6
BREV	18	1.8	1.1	0.1	5
NLCD	22	1.7	1.5	0.04	6
BRCD	32	1.8	1.5	0.06	6
C3GR	27	1.8	1.3	0.06	6
C4GR	27	1	2	0.06	15

Table 20.2. Mapping of SiB land cover type (Loveland et al., 2000) to dominant generalized plant types (GPTs) for use in the global terrestrial simulation

Simple Biosphere (SiB) Classification	Dominant GPT
Water Bodies	Missing
Evergreen broadleaf trees	Broadleaf evergreen (BREV)
Broadleaf deciduous trees	Broadleaf cold deciduous (BRCD)
Deciduous and evergreen trees	Needleleaf evergreen (NLEV)
Evergreen needleleaf trees	Needleleaf evergreen (NLEV)
Deciduous needleleaf trees	Needleleaf cold deciduous (NLCD)
Ground cover with trees and shrubs	C_4 grass (C4GR)
Groundcover only	C_4 grass (C4GR)
Broadleaf shrubs with perennial ground cover	Broadleaf evergreen (BREV)
Broadleaf shrubs with bare soil	Broadleaf evergreen (BREV)
Groundcover with dwarf trees and shrubs	Broadleaf evergreen (BREV)
Bare soil	Bare
Agriculture or C3 grassland	C_3 herbaceous (C3GR)
Persistent wetland	Moss
Ice cap and glacier	Missing
Missing data	Missing

LAI × mean N content (Table 20.1) gives total canopy N in each pixel for each month. Foliar N is distributed over horizontal canopy layers using a simple exponential decline with canopy depth, fitted to data collected in a high canopy N tropical rainforest (Carswell et al., 2000). The ratio of chlorophyll to foliar N is assumed to increase with depth, with a relationship fitted to the data of Kull and Kruijt (1998). These relationships are described fully by Friend and Kiang (2005).

3. Environmental Forcing

The biochemical model is driven by the intercellular partial pressures of CO_2 and O_2, leaf temperature, and the flux of photosynthetically active photons penetrating the leaf. Leaf photosynthesis is integrated across sun and shade foliage in horizontal layers with thicknesses of 0.5 LAI units at a 30 min timestep to give canopy photosynthesis. Intercellular O_2 is assumed constant at 20.9 kPa,

but CO_2 is calculated from the balance of fixation in chloroplasts, respiration from mitochondria, and diffusion through the stomatal pores (permeable epidermis in the case of moss). A unique numerical solution for the mean intercellular CO_2 is obtained for the entire canopy on each timestep. Canopy stomatal conductance is calculated using the semi-empirical model described by Friend and Kiang (2005). This includes empirical responses to soil water potential, intercellular CO_2 partial pressure, intercellular to free air specific humidity gradient, and the potential rate of canopy photosynthesis under conditions of saturating CO_2 (Friend and Kiang, 2005). An effect of mean canopy height is also included, but for the simulations shown here mean canopy height is fixed at 0.5 m to avoid the need for a global canopy height dataset. Soil water potential in each soil layer is calculated from relative water content as in Friend (1995).

Foliar mitochondrial respiration is required to balance the CO_2 flux, and is calculated as a function of canopy N and temperature. The temperature response for C_3 leaves is taken from Bernacchi et al. (2001), and the response for C_4 leaves is taken from Collatz et al. (1992). N dependence of respiration is calibrated from eddy-covariance sites with different linear relationships for C_3 and C_4 physiologies.

Incoming direct and diffuse PAR is distributed over canopy layers using the scheme of Spitters et al. (1986), as implemented by Friend (2001). Canopy temperature, boundary layer transfer coefficients, and soil moisture are calculated using the land surface scheme of the NASA Goddard Institute for Space Studies global climate model II (Hansen et al., 1983), with the coefficient for CO_2 transfer assumed to equal that for sensible heat. Two soil layers are used, 0.1 and 2 m depth, and the spatial distribution of field capacity in each is calculated by aggregating the IGBP-DIS 5' dataset to ¼° (Global Soil Data Task Group, 2000). Canopy temperature is assumed to equal the temperature of the upper soil layer, and the intercellular specific humidity is assumed saturated at that temperature. Potential soil evaporation uses a soil surface resistance calculated from the relative moisture content of the upper soil layer and relative humidity at the soil surface calculate from its soil water potential (Xue et al., 1996), and is reduced as a negative exponential function of LAI. Canopy transpiration is subtracted from the soil layer with the highest relative water content, with all plant types assumed to have access to both layers.

Atmospheric forcing at 10 m above canopy top is created using a weather generator parameterized with mean-monthly fraction of wet days, precipitation per wet day, 24-h maximum and minimum temperatures, 24-h shortwave radiation, and water vapor pressure. These values are derived from the 10' CRU CL 2.0 1961–1990 mean climatology (New et al., 2002), and aggregated to ¼°. 24-h shortwave radiation is calculated from relative sunshine duration using the mean global parameterization of Friend (1998).

The weather generator described by Friend (1998) generates daily precipitation, minimum and maximum temperatures, total shortwave irradiance, and mean water vapor partial pressure. Mean daily atmospheric optical depth (AOD) is calculated from the generated daily shortwave and potential daily shortwave with no atmosphere. AOD is then assumed constant during the day and used with sun angle to estimate ½-hr values of direct and diffuse PAR using the relationships given by Spitters et al. (1986), assuming a fixed ratio of PAR to total shortwave. Atmospheric pressure, wind speed, and atmospheric CO_2 concentration are assumed constant (viz. 101325 Pa, 2 m s^{-1}, 14.1 mmol m^{-3}). Daily precipitation is spread evenly across sub-daily timesteps. A linear regression is calculated for each day between the temperature extremes and shortwave radiation. This relationship is then used to calculate air temperature at each timestep, from which water vapor mixing ratio is derived from the generated mean daily water vapor pressure. Downward longwave irradiance is parameterized as a function of cloud cover fraction and air temperature using the formulation of Pirazzini et al. (1998), with clear-sky emissivity set to 0.69, and cloud cover fraction assumed fixed at 0.8.

B. Marine Photosynthesis

Water-column integrated global ocean net primary production (NPP) was calculated using the *Carbon-based Production Model* (CbPM) as described by Westberry et al. (2008), with only

minor modifications to input data sets. The CbPM is a depth-resolved, spectral model that is unique among ocean NPP algorithms in two significant respects. First, the CbPM calculates NPP as the product of phytoplankton biomass (carbon concentration, C_{phyto}) and growth rate, μ (i.e., NPP $= \mu \times C_{phyto}$), where C_{phyto} is derived from satellite particulate backscattering coefficients (b_{bp}) and μ is derived from the ratio of satellite chlorophyll and C_{phyto} concentrations. Thus, both phytoplankton biomass and physiological variability are derived directly from remotely sensed ocean properties. This contrasts with traditional chlorophyll-based algorithms where NPP $= Chl \times P^{Chl}$ and empirical, field-based relationships are applied to describe variability in P^{Chl}. The second innovation of the CbPM is that information on surface mixing depth, depth of the nutricline, and physiological responses to light- and nutrient-conditions are used to iteratively evolve distributions of chlorophyll, light, and NPP through the water column for each satellite pixel. This approach contrasts with earlier treatments where empirical Gaussian functions based on surface chlorophyll concentration are used to describe depth-variations in chlorophyll, that are then applied to estimate water-column light- and NPP distributions.

A complete description of the CbPM approach is provided by Westberry et al. (2008), while here only a brief overview is given. Additional information on the CbPM, model code, and global products can be found on the Ocean Productivity Website at: http://science.oregonstate.edu/ocean.productivity/.

1. Underwater Light Field

Global, gridded 8-day fields of cloud-corrected PAR (Ein m^{-2} day^{-1}) incident at the sea surface and diffuse attenuation coefficients at 490 nm, $K_d(490)$, (m^{-1}), were obtained from the OceanColor Web (http://oceancolor.gsfc.nasa.gov) and based on Sea-viewing Wide Field-of-view Sensor (SeaWiFS) measurements between September 1997 and July 2007 (spatial resolution of $\sim$ 18 km at the equator). PAR was decomposed spectrally using constant fractions estimated from an atmospheric radiative transfer model (Ricchiazzi et al., 1998; Westberry et al., 2008). Spectral diffuse attenuation coefficients for the visible waveband, $K_d(\lambda)$, were calculated from $K_d(490)$ using the model of Austin and Petzold (1986). Combining these spectral irradiance and attenuation estimates permits the differential propagation of light with depth and yields an accurate characterization of the underwater light environment.

In the CbPM, $K_d(\lambda)$ is assumed to be constant within the mixed layer. Below this surface layer, chlorophyll concentration varies with depth in response to changing light and nutrient conditions (see below), which consequently alters $K_d(\lambda)$. This feedback between physiological acclimation and light attenuation is captured by iteratively propagating light through the water column (Westberry et al., 2008). For these calculations, MLD was obtained from the Ocean Productivity Website and defined as the depth at which density is 0.125 kg m^{-3} greater than the density at 10 m.

2. Phytoplankton Carbon, Chlorophyll, and Net Primary Production

Global, gridded 8-day fields of SeaWiFS normalized water leaving radiances, $nLw(\lambda)$, were obtained from the OceanColor Web and inverted using a non-linear minimization method that solves for three unknown quantities: Chl, b_{bp}, and absorption by colored dissolved matter (a_{cdm}) (Maritorena et al., 2002). Variations in b_{bp} reflect changes in particle abundance and can be related to phytoplankton carbon (C_{phyto}) because (1) the particle size spectrum in the open ocean is highly conserved, (2) phytoplankton contribute directly and significantly to b_{bp}, and (3) the concentration of individual components of the particle assemblage covaries with phytoplankton abundance (Behrenfeld and Boss, 2003, 2006; Westberry et al., 2008). In the CbPM, mixed layer C_{phyto} is calculated as:

$$C_{phyto} = 13,000 \cdot \left(b_{bp} - b_{bpNAP}\right), \qquad (20.7)$$

where b_{bpNAP} is a correction for background scattering from non-algal particles (0.00035 m^{-1}, from Westberry et al., 2008). Below the mixed layer, the vertical profile of C_{phyto} is assumed uniform and equal to the surface value up to a depth where growth rate (see below) equals

a constant and low background loss rate (0.1 day^{-1}), after which C_{phyto} decreases smoothly with depth (Westberry et al., 2008).

Chlorophyll concentration is a function of both phytoplankton biomass and physiological variability in intracellular pigmentation (i.e., *Chl*:C ratio). Under nutrient-replete conditions, *Chl*:C is a strong function of growth irradiance (I_g) and can be characterized as a decreasing exponential function of I_g. In the mixed layer, I_g is the median daily PAR for the mixing depth. Phytoplankton growth rates in the mixed layer are first described as a saturating function of I_g and then adjusted downward to account for nutrient stress effects. This adjustment is made using the difference between satellite-derived *Chl*:C and the anticipated nutrient-replete *Chl*:C value for the given mixed layer I_g value (Westberry et al., 2008).

Below the mixed layer, an iterative scheme is employed for calculating the vertical distribution of phytoplankton *Chl* and μ. With each vertical increment, the phytoplankton community acclimates to the slightly lower light level of its depth horizon by increasing intracellular pigmentation (*Chl*:C), with μ responding accordingly. This photoacclimation response is similar to that employed for the mixed layer, but is also influenced by the vertical distribution of nutrients. Specifically, depth-dependent relaxation from surface nutrient stress enhances growth rates for a given I_g (thus, increased *Chl*:C). This nutrient effect is characterized according to distance from the nitracline, where nitracline depths are provided from monthly climatological nutrient fields reported in the World Ocean Atlas (Conkright et al., 2002; Westberry et al., 2008). The vertical nutrient gradient thus allows chlorophyll concentration to increase more rapidly from the surface to the nitracline than would otherwise occur from photoacclimation alone. Below the nitracline, phytoplankton are assumed to be nutrient replete, such that continued depth-dependent changes in chlorophyll are due only to changes in light and C_{phyto}. Once this iterative process is complete, NPP at each depth (z) is calculated as:

$$\mathrm{NPP}(z) = \mu(z) \cdot C_{\mathrm{phyto}}(z) \qquad (20.8)$$

and then integrated over the water column to achieve an areal NPP estimate (mg C m^{-2} day^{-1}) for each satellite pixel.

C. Global Simulation Results

Global fields of NPP were obtained by combining the terrestrial and marine simulation results, with terrestrial NPP estimated simply as 50% of GPP. This ratio is commonly observed and is consistent with theoretical considerations (Dewar, 1996). In any case, greater complexity in modeling autotrophic respiration introduces uncertainties relative to the better-constrained photosynthesis model components due to the lack of fundamental information concerning how respiration and the processes it supports are physiologically controlled (e.g. Trumbore, 2006).

Figure 20.1 shows mean annual NPP. Global NPP is 107.3 Pg C $year^{-1}$, with 54.8 Pg C $year^{-1}$ on land and 52.5 Pg C $year^{-1}$ in the oceans. Field et al. (1998) estimated 56.4 Pg C $year^{-1}$ on land and 48.5 Pg C $year^{-1}$ in the oceans, with the latter including a 1 Pg C $year^{-1}$ contribution from macroalgae, not considered here. Differences with our simulation could be due to the time period and/or the methods. As expected, the general patterns are similar to those found in other studies, such as Field et al. (1998). However, compared to this work, boreal forest NPP is around 50% higher (at 50° N) in these new simulations, whereas tropical forest NPP is lower by ≈40% (e.g. at −10° S). The greatest differences for ocean NPP are in the southern Ocean, where the new model estimates fluxes ≈50% below those of Field et al. (1998). These lower values are compensated by higher NPP towards the equator (e.g. ≈ 40% higher at 0° N). Further work will be necessary to determine the source of these large differences, but are likely linked to improved treatment of leaf-level photosynthesis on land and of spatial and taxonomic physiological variability in the ocean. Establishing the accuracy of these simulations will need to utilize a combination of tower, sea surface, and atmospheric CO_2 concentration measurements (Friend et al., 2007).

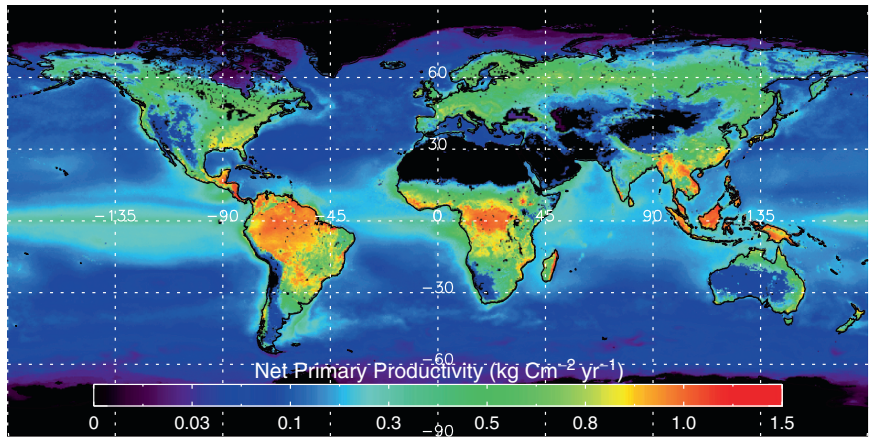

Fig. 20.1. Mean annual net primary productivity (NPP) simulated by Hybrid6.5 (land) and the CbPM (ocean) for the period 2000–2007. Total mean annual NPP is 107.3 Pg C year^{-1}, with 51.1% coming from land and 48.9% from the oceans. Land pixels simulated with $^1/_4°$ resolution and ocean pixels with $^1/_{12}°$ resolution. Land leaf area dynamics prescribed from MODIS satellite retrievals, ocean production calculated using data from the SeaWiFS instrument. Full simulation details are given in the text. See also Color Plates, Fig. 7

IV. Concluding Remarks

It is interesting to note that terrestrial and marine approaches to modelling primary production both fall into two equivalent categories, one essentially empirical (using remote sensing) and one mechanistic. Both "top-down" approaches rely on remote-sensing of the distribution of photosynthetic capacity (Chl *a* and carbon in the sea, LAI on land), and in most cases use a linear scaling with absorbed light. "Bottom-up" approaches are built using understanding of the environmental controls on capacity, and have the potential to evaluate photosynthesis outside of the period of the satellite record, using DGOMs in the case of the sea and DGVMs on land. The following section gives an overview of the issues that need to be addressed in the future to increase our confidence in this second class of model.

A. Future Challenges

1. Terrestrial Systems

Prognostic global simulations of future terrestrial photosynthesis will continue to play a major role in studies of future potential impacts of, and feedbacks on, global environmental change. However, validation of existing approaches remains a major problem. We lack key datasets for testing canopy-scale simulations of photosynthesis, partly due to the small number of sites with measurement towers and partly due to inherent methodological problems resulting in missing data and difficulty in separating photosynthesis from net ecosystem exchange. High quality datasets need to be assembled to allow precise evaluation of models, including identification of potential sources of bias such as hydrological feedbacks, canopy temperatures, and physiological attributes. It is frustrating that data constraints mean that model evaluations fail to separate bias in physics from bias in physiology. Datasets need to be assembled that contain the full range of necessary ancillary information, such as canopy nitrogen contents, temperatures, soil moisture, radiation profiles, and site history.

Current models are also poorly constrained with respect to controls on spatial and temporal variation in capacity (i.e. leaf area and nitrogen content), contributions of physiological diversity, and the potential for physiologies, populations, and species mixes to adapt to environmental change. Future projections will depend critically on how well capacity and ecosystem changes are modeled. However, most models currently treat these processes very simply, if at all. Aggregation of species into a few functional types makes parameterization easier, but it is likely that the system response to changing climate

and atmospheric CO_2 cannot be fully captured by a few fixed physiological types. The potential effects of physiological adjustment (phenotypic plasticity), competition between individuals and species with variable physiologies, and evolution need to be evaluated. These are the mechanisms whereby organisms and ecosystems maintain their viability in the face of environmental change. Identification of trade-offs between key physiological traits will make the problem of parameterization of a large number of plant types substantially easier. All these developments will require close collaborations among experimentalists and modelers.

2. Marine Systems

Development and application of ocean biogeochemical models are driven by the desire to understand how the ocean carbon cycle has responded to climate change in the past (glacial to interglacial) and how it will respond to global warming in the future. By necessity, the parameterization of biogeochemistry included in an ocean GCM must be highly simplified when compared with reality, and there will always be a tradeoff between realism and tractability. A major step forward in ocean biogeochemical models was subdividing generic phytoplankton used in early NPZD models into a small number of phytoplankton functional types used in DGOMs. However, even DGOMs employ a small number of trophic interactions, a limited amount of metabolic diversity (genotypes present), and typically neglect physiological plasticity (phenotypic response) (Hood et al., 2007). Increasing the number of phytoplankton types has raised important problems including how to validate model performance (Anderson, 2005) and how to specify parameter values (Friedrichs et al., 2007). The data needed to validate multigroup biogeochemical models may not be available, and more complex ecological models do not necessarily perform better at accounting for the variability that is seen in the existing datasets than simpler models with much more highly aggregated ecology (Anderson, 2005). Data assimilation, typically using an adjoint method, can improve estimates of parameter values (Friedrichs et al., 2007). However, the predictive skill of a tuned model depends critically upon the availability of appropriate datasets for parameter estimation and model validation (Friedrichs et al., 2007). The lack of appropriate data for calibrating bio-optical NPP algorithms has also been emphasized (Carr et al., 2006; Sathyendranath and Platt, 2007). It is likely that parameter estimation and model validation will be improved with increased use of the expanding range of products that can be retrieved from satellite observations. These include initial attempts to map pelagic calcium carbonate production (Balch et al., 2007), *Trichodesmium* blooms (Westberry and Siegel, 2006), and phytoplankton groups (Alvain et al., 2005, 2008).

Another important issue, which has not received equal attention, is how much physiological detail to include for each functional type (Flynn, 2005, 2006; Hood et al., 2007). It can be argued that the simple parameterizations of phytoplankton physiology, such as the Monod equation for limitation of growth rate by the concentration of a single limiting nutrient, need to be replaced by models that include more sophisticated treatments of the interactions amongst limiting factors and physiological acclimation (Flynn, 2005; Hood et al., 2007). Alternatively, better parameterizations of phytoplankton functional types may arise by explicitly modeling the costs and benefits of trade-offs amongst functional traits (Litchman et al., 2007) and by conducting competition experiments *in silico* in ocean GCMs (Follows et al., 2007).

New processes may need to be included in the parameterizations of phytoplankton functional types. One significant difference between marine and terrestrial models is that marine models ignore CO_2 limitation. The historical reason for this is that dissolved inorganic carbon (DIC) in seawater is not a limiting factor in the sense of Liebig's Law of the Minimum. However, the potential for CO_2 limitation of marine phytoplankton photosynthesis in the sense of Blackman's Law arises because CO_2 accounts for only about 1% of the DIC in seawater (Wolf-Gladrow et al., 1999). Although CO_2 limitation is suppressed in many algae and cyanobacteria by biophysical CO_2 concentration mechanisms (Giordano et al., 2005), reductions of growth rate with reductions of p_{CO2} below ambient levels have been reported for some diatoms (Riebesell et al., 1993). There is also evidence that CO_2 availability affects competition within the phytoplankton community (Tortell

et al., 2002). Perhaps the most significant recent finding is that N_2 fixation and growth of *Trichodesmium* is sensitive to the increases in p_{CO2} that are expected to occur over the next 100 years (Hutchins et al., 2007).

In light of our rapidly increasing knowledge of the diversity of marine microbes afforded by genomic approaches, Hood et al. (2007) have concluded that "traditional modeling tools ... to simulate marine-ecosystem dynamics and biogeochemical cycles will be insufficient to allow an informed synthesis of this information...". They suggest increased use of overarching ecological theories based on thermodynamic constraints or concepts of resilience, continued development and application of physiological models, increased use of simulations of natural selection, and increased use of individual-based models to study microbial interactions. Some of these approaches can be employed within ocean GCMs, whereas others can be used to develop new parameterizations of the role of microbes in ocean biogeochemistry. However, increasing model complexity in this way will compound concerns with respect to obtaining the appropriate data for model validation.

New functional types may need to be included in models. For example, anoxygenic photoheterotrophic bacteria (Kolber et al., 2001) have been shown to be abundant and active in oligotrophic waters, which account for about 60% of the open ocean surface area (Koblizek et al., 2007; Lami et al., 2007). These organisms contain bacteriochlorophyll and have a similar photosynthetic efficiency and spectral light utilization to oxygenic phytoplankton. However, they rely on an organic carbon source, instead of water, as an electron donor. Bacteriochlorophyll is present at concentrations considerably lower than Chl *a* (Lami et al., 2007), so it is unlikely that anoxygenic photosynthesis makes a major direct contribution to marine primary production, although these photoheterotrophic bacteria may be important in other ways (Kolber et al., 2001).

Acknowledgments

ADF acknowledges the support of the Centre National de la Recherche Scientifique (France) and the European Commission through Contract Number MRTN-CT-2004-512464 (GREENCYCLES Marie Curie Research Training Network). ADF also wishes to thank Sönke Zaehle for numerous stimulating discussions on modeling primary productivity. MJB acknowledges support from the National Aeronautics and Space Administration (USA) and wishes to thank Robert O'Malley and Toby Westberry for ocean modeling contributions to this work. RJG's work on modeling marine photosynthesis is supported by the UK Natural Environment Research Council MARQUEST initiative. CJS acknowledges the support of the NASA New Investigator Program.

References

Alvain S, Moulin C, Dandonneau Y and Bréon FM (2005) Remote sensing of phytoplankton groups in case 1 waters from global SeaWiFS imagery. Deep-Sea Res Pt I 52: 1989–2004

Alvain S, Moulin C, Dandonneau Y and Loisel H (2008) Seasonal distribution and succession of dominant phytoplankton groups in the global ocean: a satellite view. Global Biogeochem Cy 22: GB3001

Amthor JS (2000) The McCree-de Wit-Penning de Vries-Thornley respiration paradigms: 30 years later. Ann Bot-London 86: 1–20

Anderson TR (2005) Plankton functional type modelling: running before we can walk? J Plankton Res 27: 1073–1081

Antoine D, Morel A, Gordon HR, Banzon VF and Evans RH (2005) Bridging ocean color observations of the 1980s and 2000s in search of long-term trends. J Geophys Res 110: C06009

Arrigo KR (2005) Marine microorganisms and global nutrient cycles. Nature 437: 349–355

Austin RW and Petzold TJ (1986) Spectral dependence of the diffuse attenuation coefficient of light in ocean waters. Opt Eng 25: 473–479

Badeck F-W (1995) Intra-leaf gradient of assimilation rate and optimal allocation of canopy nitrogen: a model on the implications of the use of homogeneous assimilation functions. Aust J Plant Physiol 22: 425–439

Balch WM, Gordon HR, Bowler BC, Drapeau DT and Booth ES (2005) Calcium carbonate measurements in the surface global ocean based on Moderate-Resolution Imaging Spectroradiometer data. J Geophys Res 110: C07001

Balch W, Drapeau D, Bowler B and Booth E (2007) Prediction of pelagic calcification rates using satellite measurements. Deep-Sea Res Pt II 54: 478–495

Baldocchi DD and Wilson KB (2001) Modeling CO_2 and water vapor exchange of a temperate broadleaved forest across to decadal time series. Ecol Modell 142: 155–184

Ball JT, Woodrow IE and Berry JA (1987) A model predicting stomatal conductance and its contribution to the control of photosynthesis under different environmental conditions. In: Biggins J (ed) Progress in Photosynthesis Research, Vol IV, pp. 221–224. Martinus Nijhoff, Dordrecht, The Netherlands

Banse K and Postel JR (2003) On using pigment-normalized, light-saturated carbon uptake with satellite-derived pigment for estimating column photosynthesis. Global Biogeochem Cy 17: 1079

Behrenfeld MJ and Boss E (2003) The beam attenuation to chlorophyll ratio: an optical index of phytoplankton photoacclimation in the surface ocean? Deep-Sea Res Pt I 50: 1537–1549

Behrenfeld MJ and Boss E (2006) Beam attenuation and chlorophyll concentration as alternative optical indices of phytoplankton biomass. J Mar Res 64: 431–451

Behrenfeld MJ and Falkowski PG (1997a) Photosynthetic rates derived from satellite-based chlorophyll concentration. Limnol Oceanogr 41: 1–20

Behrenfeld MJ and Falkowski PG (1997b) A consumer's guide to phytoplankton primary productivity models. Limnol Oceanogr 42: 1479–1491

Behrenfeld MJ, Bale AJ, Kolber ZS, Aiken J and Falkowski PG (1996) Confirmation of iron limitation of phytoplankton photosynthesis in the equatorial Pacific Ocean. Nature 383: 508–511

Behrenfeld MJ, Boss E, Siegel DA and Shea DM (2005) Carbon-based ocean productivity and phytoplankton physiology from space. Global Biogeochem Cy 19: GB1006

Berline L, Brankart JM, Brasseur P, Ourmieres Y and Verron J (2007) Improving the physics of a coupled physical-biogeochemical model of the North Atlantic through data assimilation: Impact on the ecosystem. J Marine Syst 64: 153–172

Bernacchi CJ, Singsass EL, Pimentel C, Portis Jr AR and Long SP (2001) Improved temperature response functions for models of Rubisco-limited photosynthesis. Plant Cell Environ 24: 253–259

Berry JA and Farquhar GD (1978) The CO_2 concentration function of C_4 photosynthesis: a biochemical model. In: Hall D, Coombs J and Goodwin T (eds) Proceedings of the 4th International Congress on Photosynthesis, pp. 119–131. Biochemical Society, London

Betts RA, Cox PM, Lee SE and Woodward FI (1997) Contrasting physiological and structural vegetation feedbacks in climate change simulations. Nature 387: 796–799

Bonan GB, Levis S, Sitch S, Vertenstein M and Oleson KW (2003) A dynamic global vegetation model for use with climate models: Concepts and description of simulated vegetation dynamics. Global Change Biol 9: 1543–1566

Bond-Lamberty B and Gower S (2007) Estimation of stand-level leaf area for boreal bryophytes. Oecologia 157: 584–592

Borges AV, Delille B and Frankignoulle M (2005) Budgeting sinks and sources of CO_2 in the coastal ocean: Diversity of ecosystem counts. Geophys Res Lett 32: L1460

Botta A, Viovy N, Ciais P, Friedlingstein P and Monfray P (2000) A global prognostic scheme of leaf onset using satellite data. Global Change Biol 6: 709–725

Boyd PW, Crossley AC, DiTullio GR, Griffiths FB, Hutchins DA, Queguiner B, Sedwick PN and Trull TW (2001) Control of phytoplankton growth by iron supply and irradiance in the subantarctic Southern Ocean: Experimental results from the SAZ Project. J Geophys Res 106: 31573–31583

Bricaud A, Claustre H, Ras J and Oubelkheir K (2004) Natural variability of phytoplanktonic absorption in oceanic waters: Influence of the size structure of algal populations. J Geophys Res 109: C11010

Bricaud A, Mejia C, Blondeau-Patissier D, Claustre H, Crepon M and Thiria S (2007) Retrieval of pigment concentrations and size structure of algal populations from their absorption spectra using multilayered perceptrons. Appl Optics 46: 1251–1260

Brix H, Gruber N, Karl DM and Bates NR (2006) On the relationships between primary, net community, and export production in subtropical gyres. Deep-Sea Res Pt II 53: 698–717

Brovkin V, Ganopolski A and Svirezhev Y (1997) A continuous climate-vegetation classification for use in climate-biosphere studies. Ecol Modell 101: 251–261

Brown RH (1999) Agronomic implications of C_4 photosynthesis. In: Sage RF and Monson RK (eds) C_4 Plant Biology, pp. 473–507. Academic, San Diego, CA

Canadell JG, Le Quéré C, Raupach MR, Field CB, Buitenhuis ET, Ciais P, Conway TJ, Gillett NP, Houghton RA and Marland G (2007) Contributions to accelerating atmospheric CO_2 growth from economic activity, carbon intensity, and efficiency of natural sinks. Proc Natl Acad Sci USA 104: 18866–18870

Capone CG, Burns JA, Montoya JP, Subramaniam A, Mahaffey C, Gunderson T, Michaels AF and Carpenter EJ (2005) Nitrogen fixation by *Trichodesmium* spp.: An important source of new nitrogen to the tropical and subtropical North Atlantic Ocean. Global Biogeochem Cy 19: GB2024

Carr M-E, Friedrichs MAM, Schmeltz M, Aita MN, Barber R, Behrenfeld M, Bidigare R, Buitenhuis ET, Campbell J, Ciotti A, Dierssen H, Dowell M, Dunne J, Esaias W, Gentili B, Gregg W, Groom S, Hoepffner N, Ishizaka J, Kameda T, Le Quéré C, Lohrenz S, Marra J, Mélin F, Moore K, Morel A, Reddy TE, Ryan J, Scardi M, Smyth T, Turpie K, Tilstone G, Waters K and Yamanaka Y (2006) A comparison of global estimates of marine primary production from ocean color. Deep-Sea Res Pt II 53: 741–770

Carswell FE, Meir P, Wandelli EV, Bonates LCM, Kruijt B, Barbosa EM, Nobre AD, Grace J and Jarvis PG (2000) Photosynthetic capacity in a central Amazonian rain forest. Tree Physiol 20: 179–186

Choudhury BJ (2001) Estimating gross photosynthesis using satellite and ancillary data: approach and preliminary results. Remote Sens Environ 75: 1–25

Collatz GJ, Ball JT, Grivet C and Berry JA (1991) Physiological and environmental regulation of stomatal conductance, photosynthesis and transpiration: A model that includes a laminar boundary layer. Agr Forest Meteorol 54: 107–136

Collatz GJ, Ribas-Carbo M and Berry JA (1992) Coupled photosynthesis-stomatal conductance model for leaves of C_4 plants. Aust J Plant Physiol 19: 519–538

Collatz GJ, Berry JA and Clark JS (1998) Effects of climate and atmospheric CO_2 partial pressure on the global distribution of C_4 grasses: Present, past, and future. Oecologia 114: 441–454

Collins SL, Knapp AK, Briggs JM, Blair JM and Steinauer EM (1998) Modulation of diversity by grazing and mowing in native tallgrass prairie. Science 280: 745–747

Conkright ME, Garcia HE, O'Brien TD, Locarnini RA, Boyer TP, Stephens C and Antonov JI (2002) World Ocean Atlas 2001. Volume 4: Nutrients. Levitus S (ed) NOAA Atlas NESDID 52, US Government Printing Office, Washington, DC de Baar HJW, Boyd PW, Coale KH, Landry MR, Tsuda A, Assmy P, Bakker DCE, Bozec Y, Barber RT, Brzezinski MA, Buesseler KO, Boye M, Croot PL, Gervais F, Gorbunov MY, Harrison PJ, Hiscock WT, Laan P, Lancelot C, Law CS, Levasseur M, Marchetti A, Millero FJ, Nishioka J, Nojiri Y, Van Oijen T, Riebesell U, Rijkenberg MJA, Saito H, Takeda S, Timmermans KR, Veldhuis MJW, Waite AM and Wong C-S (2005) Synthesis of iron fertilization experiments: From the Iron Age in the Age of Enlightenment. J Geophys Res 110, C09S16

Cox PM, Betts RA, Jones CD, Spall SA and Totterdell IJ (2000) Acceleration of global warming due to carbon-cycle feedbacks in a coupled climate model. Nature 408: 184–187

Cullen JJ, Yang X and MacIntyre HL (1992) Nutrient limitation of marine photosynthesis. In: Falkowski PG and Woodhead AV (eds) Primary Productivity and Biogeochemical Cycles in the Sea, pp 69–88. Plenum Press, New York

Demarty J, Chevallier F, Friend AD, Viovy N, Piao S and Ciais P (2007) Assimilation of global MODIS leaf area index retrievals within a terrestrial biosphere model. Geophys Res Lett 34: L15402

Deutsch C, Sarmiento JL, Sigman DM, Gruber N and Dunne JP (2007) Spatial coupling of nitrogen inputs and losses in the ocean. Nature 445: 163–167

Dewar RC (1996) The correlation between plant growth and intercepted radiation: An interpretation in terms of optimal plant nitrogen content. Ann Bot-London 78: 125–136

Dickinson RE, Shaikh M, Bryant R and Graumlich L (1998) Interactive canopies for a climate model. J Climate 11: 2823–2836

Doney SC, Keith LK and Moore JK (2003) Global Ocean Carbon Cycle Modeling. In: Fasham MFR (ed) Ocean Biogeochemistry: The Role of the Ocean Carbon Cycle in Global Change, pp 217–238. Springer, Berlin/Heidelberg/New York

Duarte CM and Cebrián J (1996) The fate of marine autotrophic production. Limnol Oceanogr 41: 1758–1766

Duce RA, LaRoche J, Altieri K, Arrigo KR, Baker AR, Capone DG, Cornell S, Dentener F, Galloway J, Ganeshram RS, Geider RJ, Jickells T, Kuypers MM, Langlois R, Liss PS, Liu SM, Middelburg JJ, Moore CM, Nickovic S, Oschlies A, Pedersen T, Prospero J, Schlitzer R, Seitzinger S, Sorensen LL, Uematsu M, Ulloa O, Voss M, Ward B and Zamora L (2008) Impacts of atmospheric anthropogenic nitrogen on the open ocean. Science 320: 893–897

Dunne JP, Sarmiento JL and Gnanadesikan A (2007) A synthesis of global particle export from the surface ocean and cycling through the ocean interior and on the seafloor. Global Biogeochem Cy 21: GB4006

Falkowski PG (1997) Evolution of the nitrogen cycle and its influence on the biological sequestration of CO_2 in the ocean. Nature 387: 272–275

Falkowski PG and Kiefer DA (1985) Chlorophyll a fluorescence in phytoplankton: relationship to photosynthesis and biomass. J Plankton Res 7: 715–731

Falkowski PG and Raven JA (2007) Aquatic Photosynthesis. 2nd Edition. Princeton University Press, Princeton, NJ

Farquhar GD, Von Caemmerer S and Berry JA (1980) A biochemical model of photosynthetic CO_2 assimilation in leaves of C_3 species. Planta 149: 78–90

Farquhar GD, Ehleringer JR and Hubick KT (1989) Carbon isotope discrimination and photosynthesis. Annu Rev Plant Phys 40: 503–537

Fasham MJR, Ducklow HW and McKelvie SM (1990) A nitrogen-based model of plankton dynamics in the oceanic mixed layer. J Mar Res 48: 591–639

Field C and Mooney HA (1986) The photosynthesis-nitrogen relationship in wild plants. In: Givnish TJ (ed) On the Economy of Plant Form and Function, pp. 25–55. Cambridge University Press, Cambridge, UK

Field CB, Randerson JT and Malmström CM (1995) Global net primary production: Combining ecology and remote sensing. Remote Sens Environ 51: 74–88

Field CB, Behrenfeld MJ, Randerson JT and Falkowski P (1998) Primary production of the biosphere: Integrating terrestrial and oceanic components. Science 281: 237–240

Flynn KJ (2005) Castles built on sand: Dysfunctionality in plankton models and the inadequacy of dialogue between biologists and modellers. J Plankton Res 27: 1205–1210

Flynn KJ (2006) Reply to Horisons Article 'Plankton functional type modeling: Running before we can walk' Anderson (2005): II Putting trophic functionality into plankton functional types. J Plankton Res 28: 873–875

Foley JA, Prentice IC, Ramankutty N, Levis S, Pollard D, Sitch S and Haxeltine A (1996) An integrated biosphere model and land surface processes, terrestrial carbon bal-

ance, and vegetation dynamics. Global Biogeochem Cy 10: 603–628

Foley JA, Levis S, Prentice IC, Pollard D and Thompson SL (1998) Coupling dynamic models of climate and vegetation. Global Change Biol 4: 561–579

Follows M and Dutkiewicz S (2001) Meteorological modulation of the North Atlantic spring bloom. Deep-Sea Res Pt II 49: 321–344

Follows MJ, Dutkiewicz S, Scott Grant S and Chisholm SW (2007) Emergent biogeography of microbial communities in a model ocean. Science 315: 1843–1846

Friedlingstein P, Joel G, Field CB and Fung IY (1999) Toward an allocation scheme for global terrestrial carbon models. Global Change Biol 5: 755–770

Friedlingstein P, Bopp L, Rayner P, Cox P, Betts R, Jones C, Von Bloh W, Brovkin V, Cadule P, Doney S, Eby M, Matthews HD, Weaver AJ, Fung I, John J, Bala G, Joos F, Strassmann K, Kato T, Kawamiya M, Yoshikawa C, Knorr W, Lindsay K, Matthews HD, Raddatz T, Reick C, Roeckner E, Schnitzler K-G, Schnur R and Zeng N (2006) Climate-carbon cycle feedback analysis: Results from the C^4MIP model intercomparison. J Climate 19: 3337–3353

Friedrichs MAM, Dusenberry JA, Anderson LA, Armstrong RA, Chai F, Christian JR, Doney SC, Dunne J, Fujii M, Hood R, McGillicuddy DJ, Moore JK, Schartau M, Spitz YH and Wiggert JD (2007) Assessment of skill and portability in regional marine biogeochemical models: Role of multiple planktonic groups. J Geophys Res 112: C08001

Friend AD (1995) PGEN: An integrated model of leaf photosynthesis, transpiration, and conductance. Ecol Modell 77: 233–255

Friend AD (1998) Parameterisation of a global daily weather generator for terrestrial ecosystem modeling. Ecol Modell 109: 121–140

Friend AD (2001) Modelling canopy CO_2 fluxes: Are 'big-leaf' simplifications justified? Global Ecol Biogeogr 10: 603–619

Friend AD and Kiang NY (2005) Land surface model development for the GISS GCM: Effects of improved canopy physiology on simulated climate. J Climate 18: 2883–2902

Friend AD and White A (2000) Evaluation and analysis of a dynamic terrestrial ecosystem model under pre-industrial conditions at the global scale. Global Biogeochem Cy 14: 1173–1190

Friend AD, Stevens AK, Knox RG and Cannell MGR (1997) A process-based, terrestrial biosphere model of ecosystem dynamics (Hybrid v3.0). Ecol Modell 95: 249–287

Friend, AD, Arneth A, Kiang NY, Lomas M, Ogée J, Rödenbeck C, Running SW, Santaren J-D, Sitch S, Viovy N, Woodward FI and Zaehle S (2007) FLUXNET and modelling the global carbon cycle. Global Change Biol 13: 610–633

Fung IY, Doney SC, Lindsay K and John J (2005) Evolution of carbon sinks in a changing climate. Proc Natl Acad Sci USA 102: 11201–11206

Gattuso JP, Frankignoulle M and Wollast R (1998) Carbon and carbonate metabolism in coastal aquatic ecosystems. Annu Rev Ecol Syst 29: 405–434

Gattuso JP, Gentili B, Duarte CM, Kleypas JA, Middelburg JJ and Antoine D (2006) Light availability in the coastal ocean: Impact on the distribution of benthic photosynthetic organisms and their contribution to primary production. Biogeochemistry 3: 489–513

Geider RJ (1990) The relationship between steady state phytoplankton growth and photosynthesis. Limnol Oceanogr 35: 971–972

Geider RJ (1992) Respiration: Taxation without representation. In: Falkowski PG and Woodhead AV (eds) Primary Productivity and Biogeochemical Cycles in the Sea, pp 333–360. Plenum Press, New York

Geider RJ, MacIntyre HL and Kana TM (1998) A dynamic regulatory model of phytoplankton acclimation to light, nutrients and temperature. Limnol Oceanogr 43: 679–694

Ginoux M, Chin I, Tegen J, Prospero M, Holben B, Dubovik O and Lin SJ (2001) Sources and distributions of dust aerosols simulated with the GOCART model. J Geophys Res 106: 20255–20273

Giordano M, Beardall J and Raven JA (2005) CO_2 concentrating mechanisms in algae: Mechanisms, environmental modulation, and evolution. Annu Rev Plant Biol 56: 99–131

Global Soil Data Task Group (2000) Global Gridded Surfaces of Selected Soil Characteristics (IGBP-DIS). [Global Gridded Surfaces of Selected Soil Characteristics (International Geosphere-Biosphere Programme - Data and Information System)]. Data set. Available on-line [http://www.daac.ornl.gov] from Oak Ridge National Laboratory Distributed Active Archive Center, Oak Ridge, Tennessee, U.S.A.

Goetz SJ and Prince SD (1998) Variability in carbon exchange and light utilization among boreal forest stands: Implications for remote sensing of net primary production. Can J Forest Res 28: 37–389

Gower ST, Kucharik CJ and Norman JM (1999) Direct and indirect estimation of leaf area index, f_{apar}, and net primary production of terrestrial ecosystems. Remote Sens Environ 70: 29–51

Gregg WW (2008) Assimilation of SeaWiFS ocean chlorophyll data into a three-dimensional global ocean model. J Marine Syst 69: 205–225

Gregg WW and Casey NW (2004). Global and regional evaluation of the SeaWiFS chlorophyll data set. Remote Sens Environ 93: 463–479

Gregg WW and Casey NW (2007a) Modeling coccolithophores in the global oceans. Deep-Sea Res Pt II 54: 447–477

Gregg WW and Casey NW (2007b) Sampling biases in MODIS and SeaWiFS ocean chlorophyll data. Remote Sens Environ 111: 25–35

Gu L, Baldocchi D, Verma SB, Black TA, Vesala T, Falge EM and Dowty PR (2002) Advantages of diffuse radiation for terrestrial ecosystem productivity. J Geophys Res 107: NO. D6, 4050

Hanan NP, Berry JA, Verma SB, Walter-Shea EA, Suyker AE, Burba GG and Denning AS (2005) Testing a model of CO_2, water and energy exchange in Great Plains tallgrass prairie and wheat ecosystems. Agr Forest Meteorol 131: 162–179

Hansen J, Russell G, Rind D, Stone P, Lacis A, Lebedeff S, Ruedy R and Travis L (1983) Efficient three-dimensional global models for climate change studies: Models I and II. Mon Weather Rev 111: 609–662

Harley PC, Thomas RB, Reynolds JF and Strain BR (1992) Modelling photosynthesis of cotton grown in elevated CO_2. Plant Cell Environ 15: 271–282

Hood RR, Laws EA, Armstrong RA, Bates NR, Brown CW, Carlson CA, Chai F, Doney SC, Falkowski PG, Feely RA, Friedrichs MAM, Landry MR, Keith Moore J, Nelson D,M, Richardson TL, Salihoglu B, Schartau M, Toole DA and Wiggert JD (2006) Pelagic functional group modeling: Progress, challenges and prospects. Deep-Sea Res Pt II 53: 459–512

Hood RR, Laws EA, Follows MJ and Siegel DA (2007) Modeling and prediction of marine microbial populations in the genomic era. Oceanography 20: 155–167

Hunt Jr ER, Piper SC, Nemani R, Keeling CD, Otto RD and Running SW (1996) Global net carbon exchange and intra-annual atmospheric CO_2 concentrations predicted by an ecosystem process model and three-dimensional atmospheric transport model. Global Biogeochem Cy 10: 431–456

Huot Y, Babin M, Bruyant F, Grob C, Twardowski MS and Claustr H (2007) Relationship between photosynthetic parameters and different proxies of phytoplankton biomass in the subtropical ocean. Biogeosciences 4: 853–868

Hutchins DA, Fu FX, Zhang Y, Warner ME, Feng Y, Portune K, Bernhardt PW and Mulholland MR (2007) CO_2 control of *Trichodesmium* N_2 fixation, photosynthesis, growth rates, and elemental ratios: Implications for past, present, and future ocean biogeochemistry. Limnol Oceanogr 52: 1293–1304

Jeffrey SW, Mantoura RFC and Wright SW (1997) Phytoplankton Pigments in Oceanography: Guidelines to Modern Methods. UNESCO, Paris, France

Jenkins JP, Richardson AD, Braswell BH, Ollinger SV, Hollinger DY and Smith M-L (2007) Refining light-use efficiency calculations for a deciduous forest canopy using simultaneous tower-based carbon flux and radiometric measurements. Agr Forest Meteorol 143: 64–79

Jickells TD, An ZS, Andersen KK, Baker AR, Bergametti G, Brooks N, Cao JJ, Boyd PW, Duce RA, Hunter KA, Kawahata H, Kubilay N, LaRoche J, Liss PS, Mahowald N, Prospero JM, Ridgwell AJ, Tegen I and Torres R (2005) Global iron connections between desert dust, ocean biogeochemistry, and climate. Science 308: 67–71

Justice CO, Townshend JRG, Holben BN and Tucker CJ (1985) Phenology of global vegetation using meteorological satellite data. Int J Remote Sens 8: 1271–1318

Kaduk J and Heimann M (1996) A prognostic phenology scheme for global terrestrial carbon cycle models. Climate Res 6: 1–19

Kamykowski D, Zentara SJ, Morrison JM and Switzer AC (2002) Dynamic global patterns of nitrate, phosphate, silicate, and iron availability and phytoplankton community composition from remote sensing data. Global Biogeochem Cy 16: NO. 4, 1077

Kathuroju N, White MA, Symanzik J, Schwartz MD, Powell JA and Nemani RR (2007) On the use of the advanced very high resolution radiometer for development of prognostic land surface phenology models. Ecol Modell 201: 144–156

Knops JMH and Reinhart K (2000) Specific leaf area along a nitrogen fertilization gradient. Am Midl Nat 144: 265–272

Knorr W and Kattge J (2005) Inversion of terrestrial ecosystem model parameter values against eddy covariance measurements by Monte Carlo sampling. Global Change Biol 11: 1333–1351

Koblizek M, Masin M, Ras J, Poulton AJ and Prášil O (2007) Rapid growth rates of aerobic anoxygenic phototrophs in the ocean. Environ Microbiol 9: 2401–2406

Kolber ZS, Plumley FG, Lang AS, Beatty JT, Blankenship RE, VanDover CL, Vetriani C, Koblizek M, Rathgeber C and Falkowski PG (2001) Contribution of aerobic photoheterotrophic bacteria to the carbon cycle in the ocean. Science 292: 2492–2495

Krinner G, Viovy N, de Noblet-Ducoudré N, Ogée J, Polcher J, Friedlingstein P, Ciais P, Sitch S and Prentice IC (2005) A dynamic global vegetation model for studies of the coupled atmosphere-biosphere system. Global Biogeochem Cy 19: GB1015

Kucharik CJ, Foley JA, Delire C, Fisher VA, Coe MT, Lenters JD, Young-Molling C and Ramankutty N (2000) Testing the performance of a Dynamic Global Ecosystem Model: Water balance, carbon balance, and vegetation structure. Global Biogeochem Cy 14: 795–825

Kucharik CJ, Barford CC, El Maayar M, Wofsy SC, Monson RK and Baldocchi DD (2006) A multiyear evaluation of a Dynamic Global Vegetation Model at three Ameriflux forest sites: Vegetation structure, phenology, soil temperature, and CO_2 and H_2O vapor exchange. Ecol Modell 196: 1–31

Kull O and Kruijt B (1998) Leaf photosynthetic light response: A mechanistic model for scaling photosynthesis to leaves and canopies. Funct Ecol 12: 767–777

Lami R, Cottrell MT, Ras J, Ulloa O, Obernosterer I, Claustre H, Kirchman DL and Lebaron P (2007) High abundances of aerobic anoxygenic photosynthetic bacteria in the South Pacific Ocean. Appl Environ Microbiol 73: 4198–4205

Lapeyre G and Klein P (2006) Impact of the small-scale elongated filaments on the oceanic vertical pump. J Mar Res 64: 835–851

Laws EA, Falkowski PG, Smith WO, Ducklow H and McCarthy JJ (2000a) Temperature effects on export production in the open ocean. Global Biogeochem Cy 14: 1231–1246

Laws EA, Landry MR, Barber RT, Campbell L, Dickson ML and Marra J (2000b) Carbon cycling in primary production bottle incubations: Inferences from grazing experiments and photosynthetic studies using C-14 and O-18 in the Arabian Sea. Deep-Sea Res Pt II 47: 1339–1352

Le Quéré C, Harrison SP, Prentice IC, Buitenhuis ET, Aumont O, Bopp L, Claustre H, Cotrim Da Cunha L, Geider R, Giraud X, Klaas C, Kohfeld KE, Legendre L, Manizza M, Platt T, Rivkin RB, Sathyendranath S, Uitz J, Watson AJ and Wolf-Gladrow D (2005) Ecosystem dynamics based on plankton functional types for global ocean biogeochemistry models. Global Change Biol 11: 2016–2040

Leuning R (1995) A critical appraisal of a coupled stomatal-photosynthesis model for C_3 plants. Plant Cell Environ 18: 339–355

Litchman E, Klausmeier CA, Schofield OM and Falkowski PG (2007) The role of functional traits and trade-offs in structuring phytoplankton communities: Scaling from cellular to ecosystem level. Ecol Lett 10: 1170–1181

Liu X-Y, Xiao H-Y, Liu C-Q and Li Y-Y (2007) $\delta^{13}C$ and $\delta^{15}N$ of moss *Haplocadium microphyllum* (Hedw.) Broth. for indicating growing environment variation and canopy retention on atmospheric nitrogen deposition. Atmos Environ 41: 4897–4907

Lloyd J, Bird MI, Veenendaal E and Kruijt B (2001) Should phosphorus availability be constraining moist tropical forest responses to increasing CO_2 concentrations? In: Schulze E-D, Harrison SP, Heimann M, Holland EA, Lloyd J, Prentice IC and Schimel D (eds) Global Biogeochemical Cycles in the Climate System, pp 96–114. Academic, San Diego, CA, USA

Lobell BD, Hicke JA, Asner GP, Field CB, Tucker CJ and Los O (2002) Satellite estimates of productivity and light use efficiency in United States agriculture, 1982–98. Global Change Biol 8: 722–735

Long SP (1999) Environmental responses. In: Sage RF and Monson RK (eds) C_4 Plant Biology, pp. 215–249. Academic, San Diego, CA

Longhurst A, Sathyendranath S, Platt T and Caverhill C (1995) An estimate of global primary production in the ocean from satellite radiometer data. J Plankton Res 17: 1245–1271

Loveland TR, Reed BC, Brown JF, Ohlen DO, Zhu Z, Yang L and Merchant JW (2000) Development of a global land cover characteristics database and IGBP DISCover from 1 km AVHRR data. Int J Remote Sens 21: 1303–1330

MacIntyre HL, Kana TM, Anning T and Geider RJ (2002) Photoacclimation of photosynthesis irradiance response curves and photosynthetic pigments in microalgae and cyanobacteria. J Phycol 38: 17–38

Maritorena S, DA Siegel and AR Peterson (2002) Optimization of a semianalytical ocean color model for global-scale applications. Appl Optics 41: 2705–2714

Marrari M, Hu CM and Daly K (2006) Validation of SeaWiFS chlorophyll a concentrations in the Southern Ocean: A revisit. Remote Sens Environ 105: 367–375

Martínez-Sánchez JL (2003) Nitrogen and phosphorus resorption in trees of a neotropical rain forest. J Trop Ecol 19: 465–468

McGillicuddy DJ, Robinson AR, Siegel DA, Jannasch HW, Johnson R, Dickeys T, McNeil J, Michaels AF and Knap AH (1998) Influence of mesoscale eddies on new production in the Sargasso Sea. Nature 394: 263–266

McGillicuddy Jr DJ, Anderson LA, Doney SC and Maltrud ME (2003) Eddy-driven sources and sinks of nutrients in the upper ocean: Results from a 0.1 degrees resolution model of the North Atlantic. Global Biogeochem Cy 17: NO. 2, 1035

McGillicuddy Jr DJ, Anderson LA, Bates NR, Bibby T, Buesseler KO, Carlson CA, Davis CS, Ewart C, Falkowski PG, Goldthwait SA, Hansell DA, Jenkins WJ, Johnson R, Kosnyrev VK, Ledwell JR, Li QP, Siegel DA and SteinbergDK (2007) Eddy/wind interactions stimulate extraordinary mid-ocean plankton blooms. Science 316: 1021–1026

McGuire AD, Sitch S, Clein JS, Dargaville R, Esser G, Foley J, Heimann M, Joos F, Kaplan J, Kicklighter DW, Meier RA, Melillo JM, Moore B, Prentice IC, Ramankutty N, Reichenau T, Schloss A, Tian H, Williams LJ and Wittenberg U (2001) Carbon balance of the terrestrial biosphere in the twentieth century: Analyses of CO_2, climate and land use effects with four process-based ecosystem models. Global Biogeochem Cy 15: 183–206

McWilliam A-LC, Roberts JM, Cabral OMR, Leitao, MVBR, de Costa, ACL, Maitelli, GT and Zamparoni CAGP (1993) Leaf area index and above-ground biomass of *terra firme* rain forest and adjacent clearing in Amazonia. Funct Ecol 7: 310–317

Melillo JM, McGuire AD, Kicklighter DW, Moore B, Vorosmarty CJ and Schloss AL (1993) Global climate change and terrestrial net primary production. Nature 363: 234–240

Monteith JL (1972) Solar radiation and productivity in tropical ecosystems. J Appl Ecol 9: 747–766

Monteith JL (1977) Climate efficiency of crop production in Britain. Philos Trans R Soc B 281: 277–294

Moore JK and Doney SC (2007) Iron availability limits the ocean nitrogen inventory stabilizing feedbacks between marine denitrification and nitrogen fixation. Global Biogeochem Cy 21: GB2001

Moore JK, Doney SC and Lindsay K (2004) Upper ocean ecosystem dynamics and iron cycling in a global three-dimensional model. Global Biogeochem Cy 18: GB4028

Moore JK, Doney SC, Lindsay K, Mahowald N and Michaels AF (2006a) Nitrogen fixation amplifies the ocean biogeochemical response to decadal timescale variations in mineral dust deposition. Tellus B 58: 560–572

Moore CM, Mills, MM, Milne, A, Langlois, R, Achterberg, EP, Lochte K, Geider RJ and La Roche J (2006b) Iron supply limits primary productivity during spring bloom development in the central North Atlantic. Global Change Biol 12: 626–634

Morel A (1991) Light and marine photosynthesis: A spectral model with geochemical and climatological implications. Prog Oceanogr 26: 263–306

Morel A and Maritorena S (2001) Bio-optical properties of oceanic waters: A reappraisal. J Geophys Res 106: 7163–7180

Morel A, Antoine D, Babin M and Dandonneau Y (1996) Measured and modeled primary production in the northeast Atlantic (EUMELI JGOFS program): The impact of natural variations in photosynthetic parameters on model predictive skill. Deep-Sea Res Pt I 43: 1273–1304

Morel A, Huot Y, Gentili B, Werdell PJ, Hooker SB and Franz BA (2007) Examining the consistency of products derived from various ocean color sensors in open ocean (Case 1) waters in the perspective of a multi-sensor approach. Remote Sens Environ 111: 69–88

Morgan JA, Milchunas DG, LeCain DR, West M and Mosier AR (2007) Carbon dioxide enrichment alters plant community structure and accelerates shrub growth in the shortgrass steppe. Proc Natl Acad Sci USA 104: 14724–14729

Morisette JT, Baret F, Privette JL, Myneni RB, Nickeson JE, Garrigues S, Shabanov NV, Weiss M, Fernandes RA, Leblanc SG, Kalacska M, Sanchez-Azofeifa GA, Chubey M, Rivard B, Stenberg P, Rautiainen M, Voipio P, Manninen T, Pilant AN, Lewis TE, Iiames JS, Colombo R, Meroni M, Busetto L, Cohen WB, Turner DP, Warner ED, Petersen GW, Seufert G and Cook R (2006) Validation of global moderate-resolution LAI products: A framework proposed within the CEOS land product validation subgroup. IEEE T Geosci Remote 44: 1804–1817

Myneni RB, Keeling CD, Tucker CJ, Asrar G and Nemani RR (1997) Increased plant growth in the northern high latitudes from 1981–1991. Nature 386: 698–702

Najjar RG, Jin X, Louanchi F, Aumont O, Caldeira K, Doney SC, Dutay JC, Follows M, Gruber N, Joos F, Lindsay K, Maier-Reimer E, Matear RJ, Matsumoto K, Monfray P, Mouchet A, Orr JC, Plattner GK, Sarmiento JL, Schlitzer R, Slater RD, Weirig MF, Yamanaka Y and Yool A (2007) Impact of circulation on export production, dissolved organic matter, and dissolved oxygen in the ocean: Results from Phase II of the Ocean Carbon-cycle Model Intercomparison Project (OCMIP-2). Global Biogeochem Cy 21: GB3007

Neilson RP (1995) A model for predicting continental-scale vegetation distribution and water balance. Ecol Appl 5: 362–385

Nemani RR, Keeling CD, Hashimoto H, Jolly WM, Piper SC, Tucker CJ, Myneni RB and Running SW (2003) Climate-driven increases in global terrestrial net primary production from 1982 to 1999. Science 300: 1560–1563

New M, Lister D, Hulme M and Makin I (2002) High-resolution data set of surface climate over global land areas. Climate Res 21: 1–25

O'Reilly JE, Maritorena S, Mitchell BG, Siegel DA, Carder KL, Garver SA, Kahru M and McClain C (1998) Ocean color chlorophyll algorithms for SeaWiFS. J Geophys Res 103: 24937–24953

Orr JC, Fabry VJ, Aumont O, Bopp L, Doney SC, Feely RA, Gnanadesikan A, Gruber N, Ishida A, Joos F, Key RM, Lindsay K, Maier-Reimer E, Matear R, Monfray P, Mouchet A, Najjar RG, Plattner GK, Rodgers KB, Sabine CL, Sarmiento JL, Schlitzer R, Slater RD, Totterdell IJ, Weirig MF, Yamanaka Y and Yool A (2005) Anthropogenic ocean acidification over the twenty-first century and its impact on calcifying organisms. Nature 437: 681–686

Parton WJ, Neff J and Vitousek PM (2005) Modelling Phosphorus, Carbon and Nitrogen Dynamics in Terrestrial Ecosystems. In: Turner BL, Frossard E and Baldwin DS (eds) Organic Phosphorus in the Environment, pp. 325–334. CAB International, Oxfordshire

Pearcy RW and Ehleringer J (1984) Comparative ecophysiology of C_3 and C_4 plants. Plant Cell Environ 7: 1–13

Pirazzini R, Nardino M, Orsini A, Calzolari F, Georgiadis T and Levizzani V (1998) Parameterization of the downward longwave radiation from clear and cloudy skies at Ny Ålesund (Svalbard). Conference Presentation to the International Radiation Symposium (IRS), 24–29 July, 2000, St. Petersburg, Russia. PDF: http://www.bo.ibimet.cnr.it/fileadmin/ibimet/repository/acta13.pdf

Pitman AJ (2003) The evolution of, and revolution in, land surface schemes designed for climate models. Int J Climatol 23: 479–510

Platt T (1986) Primary production of the ocean water column as a function of surface light intensity: Algorithms for remote sensing. Deep-Sea Res 33: 149–163

Platt T, Broomhead DS, Sathyendranath S, Edwards AM and Murphy EJ (2003) Phytoplankton biomass and residual nitrate in the pelagic ecosystem. Proc R Soc A 459: 1063–1073

Polovina JJ, Howell EA and Abecassis M (2008) Ocean's least productive waters are expanding. Geophys Res Lett 35: L03618

Pons TL and Bergkotte M (1996) Nitrogen allocation in response to partial shading of a plant: Possible mechanisms. Physiol Plantarum 98: 571–577

Poorter H (1993) Interspecific variation in the growth response of plants to an elevated ambient CO_2 concentration. Vegetatio 104–105: 77–97

Popova EE, Coward AC, Nurser GA, de Cuevas B, Fasham MJR and Anderson TR (2006a) Mechanisms controlling primary production in a global ecosystem model. I: Validation of the biological simulation. Ocean Science 2: 249–266

Popova EE, Coward AC, Nurser GA, de Cuevas B and Anderson TR (2006b) Mechanisms controlling primary production in a global ecosystem model. II: The role of upper ocean short-term periodic and episodic events. Ocean Science 2: 267–279

Post WM, King AW and Wullschleger SD (1997) Historical variations in terrestrial biospheric carbon storage. Global Biogeochem Cy 11: 99–109

Potter CS, Randerson JT, Field CB, Matson PA, Vitousek PM, Mooney HA, Klooster SA (1993) Terrestrial ecosystem production: A process model based on global satellite and surface data. Global Biogeochem Cy 7: 811–841

Prince SD (1991) A model of regional primary production for use with coarse resolution satellite data. Int J Remote Sens 12: 1313–1330

Prince SD and Goward SN (1995) Global primary production: A remote sensing approach. J Biogeogr 22: 815–835

Randall DA, Dazlich DA, Zhang C, Denning AS, Sellers PJ, Tucker CJ, Bounoua L, Berry JA, Collatz GJ, Field CB, Los SO, Justice CO and Fung I (1996) A revised land surface parameterization (SiB2) for atmospheric GCMs. Part III: The greening of the Colorado State University General Circulation Model. J Climate 9: 738–763

Randerson JT, Thompson MV, Conway TJ, Fung IY and Field CB (1997) The contribution of terrestrial sources and sinks to trends in the seasonal cycle of atmospheric carbon dioxide. Global Biogeochem Cy 11: 535–560

Randerson JT, Van der Werf GR, Collatz GJ, Giglio L, Still CJ, Kasibhatla P, Miller JB, White JWC, DeFries RS and Kasischke ES (2005) Fire emissions from C_3 and C_4 vegetation and their influence on interannual variability of atmospheric CO_2 and $\delta^{13}CO_2$. Global Biogeochem Cy 19: GB2019

Ricchiazzi P, Yang SR, Gautier C and Sowle D (1998) SBDART: A research and teaching software tool for plane-parallel radiative transfer in the Earth's atmosphere. B Am Meteorol Soc 79: 2101–2114

Riebesell U, Wolf-Gladrow DA and Smetacek V (1993) Carbon dioxide limitation of marine phytoplankton growth rates. Nature 361: 249–363

Riser SC and Johnson KS (2008) Net production of oxygen in the subtropical ocean. Nature 451: 323–325

Ruimy A, Jarvis PG, Baldocchi DD and Saugier B (1995) CO_2 fluxes over plant canopies and solar radiation: A review. Adv Ecol Res 26: 1–68

Ruimy A, Kergoat L and Bondeau A (1999) Comparing global models of terrestrial net primary productivity (NPP): Analysis of differences in light absorption and light-use efficiency. Global Change Biol 5: 56–64

Running SW and Hunt Jr ER (1993) Generalization of a forest ecosystem process model for other biomes, BIOME-BGC, and an application for global-scale models. In: Ehleringer JR and Field CB (eds) Scaling physiological processes: Leaf to globe, pp. 141–158. Academic, San Diego, CA

Running SW, Nemani RR, Heinsch FA, Zhao M, Reeves M and Hashimoto H (2004) A continuous satellite-derived measure of global terrestrial primary production. Bioscience 54, 547–560

Sage RF and Monson RK (1999) C_4 Plant Biology. Academic, San Diego, CA

Sage RF, Wedin DA and Li M (1999) The Biogeography of C_4 Photosynthesis: Patterns and Controlling Factors. Academic, New York

Sarmiento JL, Slater RD, Fasham MJR, Ducklow HW, Toggweiler JR and Evans GT (1993) A seasonal three dimensional ecosystem model of nitrogen cycling in the North Atlantic euphotic zone. Global Biogeochem Cy 7: 417–450

Sathyendranath S and Platt T (1989) Remote sensing of ocean chlorophyll: Consequence of non-uniform pigment profile. Appl Optics 28: 490–495

Sathyendranath S and Platt T (2007) Spectral effects in bio-optical control on the ocean system. Oceanologia 49: 5–39

Sathyendranath S, Longhurst AR, Caverhill CM and Platt T (1995) Regionally and seasonally differentiated primary production in the North Atlantic. Deep-Sea Res Pt I 42: 1773–1802

Sato H, Itoh A and Kohyama T (2007) SEIB-DGVM: A new Dynamic Global Vegetation Model using a spatially explicit individual-based approach. Ecol Model 200: 279–307

Schmittner A, Oschlies A, Matthews HD and Galbraith ED (2008) Future changes in climate, ocean circulation, ecosystems, and biogeochemical cycling simulated for a business-as-usual CO_2 emission scenario until year 4000 AD. Global Biogeochem Cy 22: GB1013

Schwalm CR, Black TA, Amiro BD, Arain MA, Barr AG, Bourque CP-A, Dunn AL, Flanagan LB, Giasson M-A, Lafleur PM, Margolis HA, McCaughey JH, Orchansky AL and Wofsy SC (2006) Photosynthetic light use efficiency of three biomes across an east-west continental-scale transect in Canada. Agr Forest Meteorol 140: 269–286

Sellers PJ, Hall FG, Asrar G, Strebel DE and Murphy RE (1992) An overview of the First International Satellite Land Surface Climatology Project (ISLSCP) Field Experiment (FIFE). J Geophys Res 97(D17): 18345–18371

Sellers PJ, Randall DA, Collatz GJ, Berry JA, Field CB, Dazlich DA, Zhang C, Collelo GD and Bounoua L

(1996a) A revised land surface parameterization (SiB2) for atmospheric GCMs. Part I: Model formulation. J Climate 9: 676–705

Sellers PJ, Los SO, Tucker CJ, Justice CO, Dazlich DA, Collatz GJ and Randall DA (1996b) A revised land surface parameterization (SiB2) for atmospheric GCMs. Part II: The generation of global fields of terrestrial biophysical parameters from satellite data. J Climate 9: 706–737

Sharkey TD (1985) Photosynthesis in intact leaves of C_3 plants: Physics, physiology and rate limitations. Bot Rev 51: 53–105

Sigman DM and Haug GH (2003) The biological pump in the past. In: Elderfield H (ed) Treatise on Geochemistry Volume 6, pp 491–528. Elsevier, Amsterdam

Sitch S, Smith B, Prentice IC, Arneth A, Bondeau A, Cramer W, Kaplan JO, Levis S, Lucht W, Sykes MT, Thonicke K and Venevsky S (2003) Evaluation of ecosystem dynamics, plant geography and terrestrial carbon cycling in the LPJ dynamic global vegetation model. Global Change Biol 9: 161–185

Slayback DA, Pinzon JE, Los SO and Tucker CJ (2003) Northern hemisphere photosynthetic trends 1982–1999. Global Change Biol 9: 1–15

Smyth TJ, Tilstone GH and Groom SB (2005) Integration of radiative transfer into satellite models of ocean primary production. J Geophys Res 110: C10014

Spitters, CJT, Toussaint, HAJM and Goudriaan, J (1986) Separating the diffuse and direct component of global radiation and its implications for modelling canopy photosynthesis. Part I. Components of incoming radiation. Agr Forest Meteorol 38: 217–229

Stomp M, Huisman J, Voros L, Pick FR, Laamanen M, Haverkamp T and Stal LJ (2007) Colourful coexistence of red and green picocyanobacteria in lakes and seas. Ecol Lett 10: 290–298

Stramski D and Mobley CD (1997) Effects of microbial particles on oceanic optics: A database of single-particle optical properties. Limnol Oceanogr 42: 538–549

Switzer AC, Kamykowski D and Zentara SJ (2003) Mapping nitrate in the global ocean using remotely sensed sea surface temperature. J Geophys Res 108: NO. C8, 3280

Taub DR (2002) Analysis of interspecific variation in plant growth responses to nitrogen. Can J Bot 80: 34–41

Thornton PE and Zimmerman NE (2007) An improved canopy integration scheme for a land surface model with prognostic canopy structure. J Climate 20: 3902–3923

Thornton PE, Lamarque J-F, Rosenbloom NA and Mahowald NM (2007) Influence of carbon-nitrogen cycle coupling on land model response to CO_2 fertilization and climate variability. Global Biogeochem Cy 21: GB4018

Tortell PD, DiTullio GR, Sigman DM and Morel FMM (2002) CO_2 effects on taxonomic composition and nutrient utilization in an Equatorial Pacific phytoplankton assemblage. Mar Ecol-Prog Ser 236: 37–43

Trumbore S (2006) Carbon respired by terrestrial ecosystems - recent progress and challenges. Global Change Biol 12: 141–153

Tucker CJ, Townshend JRG and Goff TE (1985) African land cover classification using satellite data. Science 227: 369–375

Turner DP, Urbanski S, Bremer D, Wofsy SC, Meyers T, Gower ST and Gregory M (2003) A cross-biome comparison of daily light use efficiency for gross primary production. Global Change Biol 9: 383–395

Uitz J, Claustre H, Morel A and Hooker S (2006) Vertical distribution of phytoplankton communities in open ocean: An assessment based on surface chlorophyll. J Geophys Res 111: C08005

VEMAP Members (Melillo JM, Borchers J, Chaney J, Fisher H, Fox S, Haxeltine A, Janetos A, Kicklighter DW, Kittel TGF, McGuire AD, McKeown R, Neilson R, Nemani R, Ojima DS, Painter T, Pan Y, Parton WJ, Pierce L, Pitelka L, Prentice C, Rizzo B, Rosenbloom NA, Running S, Schimel DS, Sitch S, Smith T and Woodward, I) (1995) Vegetation/ecosystem modeling and analysis project: Comparing biogeography and biogeochemistry models in a continental-scale study of terrestrial ecosystem responses to climate change and CO_2 doubling. Global Biogeochem Cy 9: 407–437

Vitousek P (1984) Litterfall, nutrient cycling and nutrient limitation in tropical forests. Ecology 65: 285–298

Vostral CB, Boyce RL and Friedland AJ (2002) Winter water relations of New England conifers and factors influencing their upper elevational limits. I. Measurements. Tree Physiol 22: 793–800

Wand SJE, Midgley GF, Jones MH and Curtis PS (1999) Responses of wild C_4 and C_3 grass (Poaceae) species to elevated atmospheric CO_2 concentration: A meta-analytic test of current theories and perceptions. Global Change Biol 5: 723–741

Wang YP, Baldocchi D, Leuning R, Falge E and Vesala T (2007) Estimating parameters in a land-surface model by applying nonlinear inversion to eddy covariance flux measurements from eight fluxnet sites. Global Change Biol 13: 652–670

Ward BA and Waniek JJ (2007) Phytoplankton growth conditions during autumn and winter in the Irminger Sea, North Atlantic. Mar Ecol-Prog Ser 334: 47–61

Waring RH, Law BE, Goulden ML, Bassow SL, McCreight RW, Wofsy SC and Bazzaz FA (1995) Scaling gross ecosystem production at Harvard Forest with remote sensing: A comparison of estimates from a constrained quantum-use efficiency model and eddy correlation. Plant Cell Environ 18: 1201–1213

Warnant P, François L, Strivay D and Gérard J-C (1994) CARAIB: A global model of terrestrial biological productivity. Global Biogeochem Cy 8: 255–270

Wedin DA and Tilman D (1996a) Influence of nitrogen loading and species composition on the carbon balance of grasslands. Science 274: 1720–1723

Wedin DA and Tilman D (1996b) Spatial and temporal distribution of *Trichodesmium* blooms in the world's oceans. Global Biogeochem Cy 20: GB4016

Westberry T, Behrenfeld MJ, Siegel DA and Boss E (2008) Carbon-based primary productivity modeling with vertically resolved photoacclimation. Global Biogeochem Cy 22: GB2024

White MA, Thornton PE, Running SW and Nemani RR (2000) Parameterization and sensitivity analysis of the BIOME-BGC terrestrial ecosystem model: Net primary production controls. Earth Interactions 4: 1–85

Williams PJL, Morris PJ and Karl DM (2004) Net community production and metabolic balance at the oligotrophic ocean site, Station ALOHA. Deep-Sea Res Pt I 51: 1563–1578

Wolf-Gladrow DA, Riebesell U, Burkhardt S and Jelle B (1999) Direct effects of CO_2 concentration on growth and isotopic composition of marine phytoplankton. Tellus B 51: 461–476

Wong SC, Cowan IR and Farquhar GD (1979) Stomatal conductance correlates with photosynthesis capacity. Nature 282: 424–426

Wood AM (1985) Adaptation of photosynthetic apparatus of marine ultraplankton to natural light fields. Nature 316: 253–255

Woods JD and Onken R (1982) Diurnal variation and primary production in the ocean - preliminary results of a Lagrangian ensemble model. J Plankton Res 4: 735–756

Woodward FI and Lomas MR (2004) Vegetation dynamics - simulating responses to climatic change. Biol Rev 79: 643–670

Woodward FI, Smith TM and Emanuel WR (1995) A global land primary productivity and phytogeography model. Global Biogeochem Cy 9: 471–490

Wullschleger SD (1993) Biochemical limitations to carbon assimilation in C_3 plants - a retrospective analysis of the A/C_i curves from 109 species. J Exp Bot 44: 907–920

Xiao X, Melillo JM, Kicklighter DW, McGuire AD, Prinn RG, Wang C, Stone PH and Sokolov A (1998) Transient climate change and net ecosystem production of the terrestrial biosphere. Global Biogeochem Cy 12: 345–360

Xue Y, Sellers PJ, Kinter JL and Shukla J (1991) A simplified biosphere model for global climate studies. J Climate 4: 345–364

Yang W, Huang D, Tan B, Stoeve JC, Shabanov NV, Knyazikhin Y, Nemani RR and Myneni RB (2006) Analysis of leaf area index and fraction of PAR absorbed by vegetation products from the Terra MODIS sensor: 2000–2005. IEEE T Geosci Remote 44: 1829–1842

Zhao M, Heinsch FA, Nemani RR and Running SW (2005) Improvement of the MODIS terrestrial gross and net primary production global data set. Remote Sens Environ 95: 164–176